

SANDIA REPORT

SAND2022-2745

Printed March 2022



Sandia
National
Laboratories

MELCOR Accident Progression and Source Term Demonstration Calculations for a Heat Pipe Reactor

Kenneth Wagner

Chris Faucett

Rod Schmidt

David Luxat

Prepared by
Sandia National Laboratories
Albuquerque, New Mexico
87185 and Livermore,
California 94550

Issued by Sandia National Laboratories, operated for the United States Department of Energy by National Technology & Engineering Solutions of Sandia, LLC.

NOTICE: This report was prepared as an account of work sponsored by an agency of the United States Government. Neither the United States Government, nor any agency thereof, nor any of their employees, nor any of their contractors, subcontractors, or their employees, make any warranty, express or implied, or assume any legal liability or responsibility for the accuracy, completeness, or usefulness of any information, apparatus, product, or process disclosed, or represent that its use would not infringe privately owned rights. Reference herein to any specific commercial product, process, or service by trade name, trademark, manufacturer, or otherwise, does not necessarily constitute or imply its endorsement, recommendation, or favoring by the United States Government, any agency thereof, or any of their contractors or subcontractors. The views and opinions expressed herein do not necessarily state or reflect those of the United States Government, any agency thereof, or any of their contractors.

Printed in the United States of America. This report has been reproduced directly from the best available copy.

Available to DOE and DOE contractors from
U.S. Department of Energy
Office of Scientific and Technical Information
P.O. Box 62
Oak Ridge, TN 37831

Telephone: (865) 576-8401
Facsimile: (865) 576-5728
E-Mail: reports@osti.gov
Online ordering: <http://www.osti.gov/scitech>

Available to the public from
U.S. Department of Commerce
National Technical Information Service
5301 Shawnee Rd
Alexandria, VA 22312

Telephone: (800) 553-6847
Facsimile: (703) 605-6900
E-Mail: orders@ntis.gov
Online order: <https://classic.ntis.gov/help/order-methods/>



ABSTRACT

MELCOR is an integrated thermal hydraulics, accident progression, and source term code for reactor safety analysis that has been developed at Sandia National Laboratories for the United States Nuclear Regulatory Commission (NRC) since the early 1980s. Though MELCOR originated as a light water reactor (LWR) code, development and modernization efforts have expanded its application scope to include non-LWR reactor concepts. Current MELCOR development efforts include providing the NRC with the analytical capabilities to support regulatory readiness for licensing non-LWR technologies under Strategy 2 of the NRC's near-term Implementation Action Plans. Beginning with the Next Generation Nuclear Project (NGNP), MELCOR has undergone a range of enhancements to provide analytical capabilities for modeling the spectrum of advanced non-LWR concepts. This report describes the generic plant model developed to demonstrate MELCOR capabilities to perform heat pipe reactor (HPR) safety evaluations. The generic plant model is based on a publicly-available Los Alamos National Laboratory (LANL) Megapower design as modified in the Idaho National Laboratory (INL) Design A description. For plant aspects (e.g., reactor building size and leak rate) that are not described in the LANL and INL references, the analysts made assumptions needed to construct a MELCOR full-plant model. The HPR uses high assay, low-enrichment uranium (HALEU) fuel with steel cladding that uses heat pipes to transfer heat to a secondary Brayton air cycle. The core region is surrounded by a stainless-steel shroud, alumina reflector, core barrel and boron carbide neutron shield. The reactor is secured inside a below-grade cavity, with the operating floor located above the cavity. Example calculations are performed to show the plant response and MELCOR capabilities to characterize a range of accident conditions. The accidents selected for evaluation consider a range of degraded and failed modes of operation for key safety functions providing reactivity control, the primary and secondary system heat removal, and the effectiveness of the confinement natural circulation flow into the reactor cavity (i.e., a flow blockage).

ACKNOWLEDGEMENTS

This work was funded by the NRC as part of the development and demonstration activities defined in the NRC Non-Light Water Reactor Vision and Strategy Volume 3: Computer Code Development Plans for Severe Accident Progression, Source Term, and Consequence Analysis [1]. The authors gratefully acknowledge the contributions from Jason Schaperow, Hossein Esmaili, and Don Algama of the US NRC for their valuable technical guidance.

Eric Walker of Oak Ridge National Laboratory (ORNL) performed the HPR SCALE analysis and provided the radionuclide decay heat power, the radionuclide inventory, the core axial and radial power profile, and the reactivity feedbacks for this analysis. The ORNL analysis is documented in ORNL/TM-2021/2021 and is part of the same NRC-sponsored effort.

The authors gratefully recognize the contributions of Jamal Mohmand for the development of the reactor building model and Drs. Troy Haskin and Brad Beeny for their review and updates to the reactor kinetics model.

CONTENTS

1. INTRODUCTION	1
2. MELCOR HPR Modeling Features.....	3
2.1. MELCOR HPR-specific Models.....	3
2.2. MELCOR HPR Failure Models	7
3. MODEL DESCRIPTION.....	10
3.1. INL Design A HPR Overview	10
3.2. Reactor Vessel Nodalization	13
3.3. Reactor Building Nodalization.....	17
3.4. Radionuclide Inventory.....	18
3.5. Radionuclide Release Input	22
3.6. Point Kinetics Modeling.....	22
4. EXAMPLE RESULTS	23
4.1. Transient Overpower Scenario	23
4.1.1. TOP Reactor Response.....	23
4.1.2. TOP Radionuclide Response	26
4.2. Transient Overpower Scenario Sensitivity Calculations	29
4.3. Loss-of-Heat Sink and Anticipated Transient Without SCRAM	33
5. SUMMARY.....	36

LIST OF FIGURES

Figure 2-1	Illustration of a vertically oriented heat pipe.....	4
Figure 2-2	Example HP operational limits [5].	5
Figure 2-3	Example of MELCOR spent fuel pool nodalization [11].	6
Figure 2-4	Example of cascading HP nodalization.	6
Figure 2-5	Potassium Equilibrium Pressure Temperature Curve.....	8
Figure 2-6	HP failure pathways.	9
Figure 3-1	INL Design A reactor vessel cross-section [5].....	10
Figure 3-2	INL Design A reactor and secondary design schematic [12].....	11
Figure 3-3	INL Design A HP and fuel element cross-section [5].....	12
Figure 3-4	HP limit curves for the INL Design A MELCOR model using HTPIPE.....	13
Figure 3-5	INL Design A reactor vessel HP nodalization.	15
Figure 3-6	INL Design A reactor vessel volume and flow path nodalization.....	16

Figure 3-7	HPR reactor building nodalization.	18
Figure 3-8	HPR decay heat power.	19
Figure 3-9	HPR axial power profile at the beginning and end of the fuel cycle [7].	20
Figure 3-10	HPR radial power profile at the beginning and end of the fuel cycle [7].	20
Figure 4-1	Reactor power response in the TOP scenario.	25
Figure 4-2	Maximum fuel temperature response in the TOP scenario.	25
Figure 4-3	TOP scenario response on the HP performance limit graph.	26
Figure 4-4	The failed and intact HP pressure response in the TOP scenario.	28
Figure 4-5	Iodine release and distribution in the TOP scenario.	28
Figure 4-6	Iodine release pathway in the TOP scenario.	29
Figure 4-7	HP creep rupture index in the TOP scenario.	29
Figure 4-8	Iodine release to the environment the TOP sensitivity calculations.	31
Figure 4-9	Peak fuel temperature response in the ATWS and the LOHS.	34
Figure 4-10	Doppler, elongation, and expansion feedbacks in the ATWS.	35
Figure 4-11	Core power and decay heat in the ATWS.	35

LIST OF TABLES

Table 3-1	Key Parameters for the INL Design A HPR [5].	12
Table 3-2	Typical building coefficients [14].	17
Table 3-3	MELCOR radionuclide classes	21
Table 3-4	HPR radionuclide class masses.	21
Table 3-5	INL Design A reactivity feedback coefficients.	22
Table 4-1	Uncertain parameters for the HPR.	32

This page left blank

ACRONYMS AND DEFINITIONS

Abbreviation	Definition
ASHRAE	American Society of Heating, Refrigerating and Air-Conditioning Engineers
ATWS	Anticipated Transient without SCRAM
BWR	Boiling Water Reactor
COR	MELCOR core package
CV	Control Volume
HALEU	High-assay low enriched uranium
HP	Heat pipe
HPR	Heat pipe reactor
HS	Heat structure
INL	Idaho National Laboratory
LANL	Los Alamos National Laboratory
LOHS	Loss-of-heat sink
LWR	Light Water Reactor
MST	Mechanistic Source Term
NGNP	Next Generation Nuclear Plant
NRC	United States Nuclear Regulatory Commission
ORNL	Oak Ridge National Laboratory
RN	Radionuclide
SNL	Sandia National Laboratories
TOP	Transient overpower

1. INTRODUCTION

MELCOR is an integrated systems-level thermal hydraulics and source term code for reactor safety analysis [1]. It has been developed at Sandia National Laboratories for the United States Nuclear Regulatory Commission (NRC) since the early 1980s. Current MELCOR development efforts include providing the NRC with the accident analysis capabilities to support regulatory readiness for licensing non-light water reactor (non-LWR) technologies under Strategy 2 of the NRC's near-term Implementation Action Plans [2]. Beginning with the Department of Energy (DOE) Next Generation Nuclear Project (NGNP), MELCOR has undergone a range of enhancements to provide analytical capabilities for modeling the spectrum of advanced non-LWR concepts. A detailed description of the development process, including identification of technical gaps, is provided in NRC's "Non-Light Water Reactor (Non-LWR) Vision and Strategy, Volume 3 – Computer Code Development Plans for Severe Accident Progression, Source Term, and Consequence Analysis" (NRC ADAMS Accession No. ML20030A178). This report describes the generic MELCOR plant model developed to demonstrate MELCOR capabilities to perform heat pipe reactor (HPR) safety evaluations.

The MELCOR HPR model is applied to provide an example of a mechanistic source term (MST) analysis. The scope of the MST demonstration project includes development and application of a MELCOR full-plant model using publicly-available references and data. The project also includes MST demonstration calculations for other classes of non-LWR designs (e.g., high-temperature gas reactor, molten-salt-cooled pebble-bed reactor) that will be documented in separate reports.

MELCOR characterizes the evolution of the accident from the early thermal-hydraulic response through the core heat up, including the release and transport of radionuclides from the primary system to the containment or confinement buildings and to the environment [3]. The code is a knowledge repository from decades of experiments and model development with a historical focus on LWR phenomenology. However, MELCOR has been extended with new models to address non-LWR technologies.

MELCOR relies on the SCALE code system to provide the radionuclide inventories, kinetics parameters, power distributions, and decay heat, especially through the ORIGEN code. SCALE is a multi-disciplinary tool developed by ORNL for the NRC to combine nuclear system simulation tools into one cohesive package [4]. SCALE provides a comprehensive, verified and validated tool set for nuclear data, criticality safety, reactor physics, radiation shielding, radioactive source term characterization, activation, depletion and decay, and sensitivity and uncertainty analysis under a software quality assurance program. Since the 1970s, regulators, licensees, and research institutions around the world have used SCALE for safety analysis.

The MELCOR HPR input model used for the MST analysis is based on the INL Design A update [5] to the LANL Megapower design [6]. Using the data provided in the INL HPR report, a plant model of the HPR was developed. The current scope of work included (a) development of the input for the core, vessel, and heat pipes, (b) incorporation of the data from the SCALE analysis (radionuclide inventory, decay heat, and axial and radial power profiles), (c) development of a confinement building, (d) incorporation of the reactivity feedbacks, and (e) incorporation of radionuclide tracking and heat pipe failure algorithms. Section 3 describes the HPR model used in the MST calculation.

The HPR MELCOR plant model is used to simulate a transient overpower (TOP) scenario that considered a reactivity insertion due to inadvertent rotation of the reactor control drums. The

development of the input model identified gaps and uncertainties in design input data. Consequently, sensitivity calculations were performed to illustrate the relative magnitude in key figures of merit due to variations in the selected uncertainty parameters. The TOP accident progression and the source term results are described in Section 4. A second reactivity scenario is also presented that simulated an anticipated transient without SCRAM (ATWS). A summary is presented in Section 5.

This report describes the MELCOR HPR full-plant deck and its application to select scenarios. In addition, this work was presented at a public workshop on June 29, 2021 [7]. The video recording and presentation material are available at the following links:

- Video – <https://youtu.be/8pRplj75NMw>
- Slides – SCALE MELCOR HPR slides ML21179C060

2. MELCOR HPR MODELING FEATURES

The MELCOR code is organized into "packages" that correspond to different groupings of reactor regions, physics, or other code functionalities. The balance of the plant is modeled using the building block components of control volumes, heat structures, and flow paths. These basic components are used to represent primary system, the reactor vessel, the reactor building or containment, and the secondary system, which will be described for the HPR demo model in the next section. These fundamental modeling features are used for all reactor types. A unique capability of MELCOR includes an integrated calculation of radionuclide release, transport, and deposition in any problem description or nodalization.

A heat pipe (HP) works based on transferring the latent heat of vaporization of a working fluid from the evaporator region to condenser region. The nuclear heat source evaporates the working fluid in the wick of the HP. The gas flows to the condenser through the interior of the heat pipe based on the pressure gradient formed by gas generation in the evaporator at one end and gas condensation at the other end. The heat transfer from the HP wall to the secondary fluid condenses the gas on the wick adjacent to the HP wall. The liquid flows back to the evaporator along the wick due to capillary forces, and, for a vertically oriented HP, by gravity. The HP was created and demonstrated at LANL and has seen applications for space power, domestic heating, and as a demonstration HPR [8].

The level of modeling detail or discretization is user-specified based on the objectives of the analysis. An example for the LANL Megapower HPR [6] as modified in the INL Design A reactor description [5] is presented in this report. The next subsections describe some of the key MELCOR models used in the HPR demonstration calculations and an overview of the calculation solution methodology.

2.1. MELCOR HPR-specific Models

The HP geometry description and associated physics are modeled in the "COR" package. The HP COR modeling includes representation of the HP wall, the fuel and the interface between the fuel and the HP, the HP working fluid, the HP connection to the secondary heat exchanger, the HP performance limitations, and various HP failure modes.

Figure 2-1 illustrates key aspects and regions of a vertically oriented generic HP. A MELCOR HP model is specified by the key geometric attributes, which include the HP radius, the HP wall thickness, the interior wick thickness, and the porosity of the wick. The HP is subdivided into three sections: (1) the evaporator region, (2) the adiabatic region, and (3) the condenser region. Each of these HP sections are implicitly connected to specified COR package cells. Consequently, the COR nodalization for a HPR includes the active fuel region, the adiabatic region, and the condenser region. In addition, the HPR COR model includes the lower vessel head and any plenum region below the core. The HP model includes multiplicity scaling of a representative HP in the specified COR region, separate instances of HP models in other COR regions to support a discretized radial nodalization, and provisions for alternate geometry or performance criteria with multiple types of HP models. The HP model supports either sodium or potassium as the working fluid.

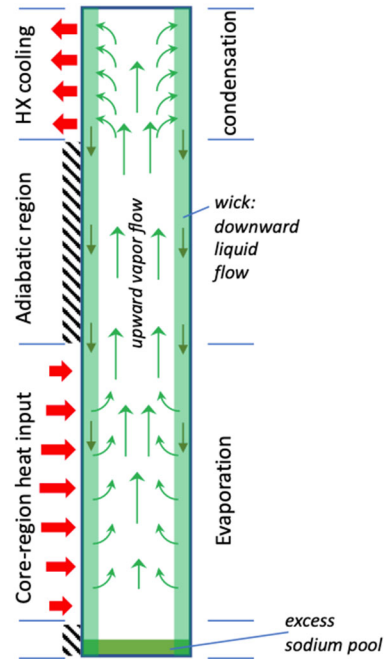


Figure 2-1 Illustration of a vertically oriented heat pipe.

The fuel adjacent to or surrounding the HPs is modeled with the fuel component. The interface between the heat pipe and the fuel is modeled with a heat conductance pathway between the fuel and the HP wall. The heat transfer connection to the condenser region is modeled between the HP wall and the fluid in the secondary side of the HP. In the adiabatic region, the model assumes no heat transfer from/to the HP outer wall.

The HP fluid remains near thermodynamic equilibrium. The equilibrium state is dynamically calculated based on the mass, volume, and enthalpy of the working-fluid in the HP. The enthalpy is used to calculate the HP pressure, temperature, and quality. The required thermodynamic properties of the working fluid (i.e., sodium or potassium) were added as part of the non-LWR model development efforts. Reference [3] provides a detailed description of the governing equations and numerical implementation.

HPs have performance limitations that can be characterized in steady state codes such as LANL's HTPIPE code [9]. There are a variety of operational limits that can constrain the performance of the heat pipe. Details of these constraints are described in the HP literature (e.g., see References [5], [9], and [10]). The MELCOR HP model includes consideration of sonic, capillary, and boiling limits. The sonic limit is associated with choked flow of the vapor through the central core. The capillary flow limit concerns the maximum liquid flow through the wick. The boiling limit concerns the onset of nucleate boiling within the evaporator section wick that degrades the heat transfer efficiency.

An example of the HP performance limits from the INL Design A report are shown in Figure 2-2, which shows the sonic, entrainment, capillary, and boiling limits. The example in Figure 2-2 includes an entrainment limit. The entrainment limit concerns liquid entrainment off the wick due to high vapor velocities, which is not more limiting than the gas phase capillary limit in this example.¹

¹ Although the MELCOR HP model only considers the sonic, capillary, and boiling limits, these responses provide a generic framework that could incorporate other failure modes. For example, if the entrainment limit was more limiting than the capillary limit, the minimum of the two could be used in the MELCOR input. The code response to

However, the HP performance limit curves are highly dependent on the HP geometry and the wick construction, the HP orientation, and the working fluid. The operating power versus fluid temperature shown in Figure 2-2 is the typical presentation of the HP limits.

Although not investigated in the scope of the current report, MELCOR has the flexibility to investigate a cascading heat pipe scenario using a locally refined nodalization. The capability originates from spent fuel pool modeling. The heat transfer pathways for the typical cylindrical ring orientation are reconfigured in MELCOR spent fuel models to reflect more complex arrangements. For example, Figure 2-3 shows a complex spent fuel pool arrangement. The color-coded fuel assemblies are associated with particular rings in the MELCOR model. The assemblies are grouped based on their offload time (i.e., decay heat power) rather than concentric cylindrical rings. The spent fuel pool arrangement shows that Ring 2 primarily surrounds Ring 1 but is also adjacent to Ring 4 on the outer periphery. The generalized heat transfer pathway model allows redefinition of the heat transfer pathways to reflect this configuration, which is essential for spent fuel pool analysis.

Figure 2-4 shows a possible approach to refining the heat pathways around a single failed HP. A single HP (i.e., the inner ring) is shown that is concentrically surrounded by the three rings. The full nodalization would continue to discretize the remaining HPs in the core with consideration of the HP power and their geometric location. There is no limit on the number of rings but the use of 10 to 30 rings is customary (e.g., see Section 3.2). The refined model allows a more accurate analysis of the heat flow surrounding a single HP. The user interface to the HP model allows specification of the HP failure based on any quantified condition (e.g., as an initial condition, at a specific time, or based on the internal HP pressure).

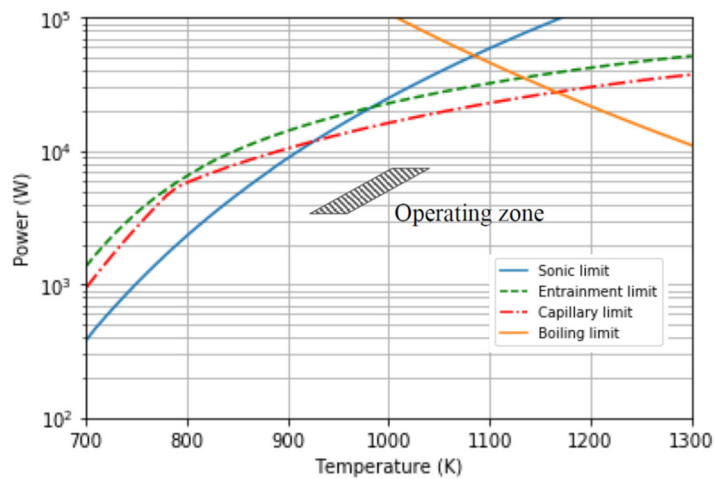


Figure 2-2 Example HP operational limits [5].

an entrainment limit could be modeled as a capillary limit, which limits the working fluid flow back to the evaporator region. Both conditions could progress to an evaporator over-heating condition.

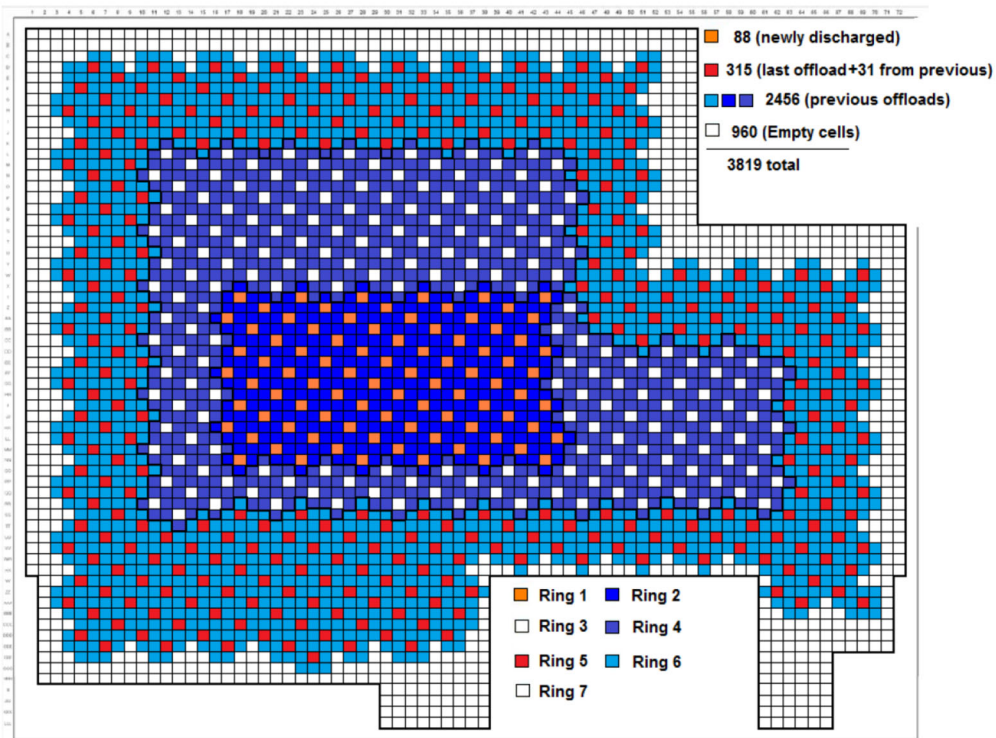


Figure 2-3 Example of MELCOR spent fuel pool nodalization [11].

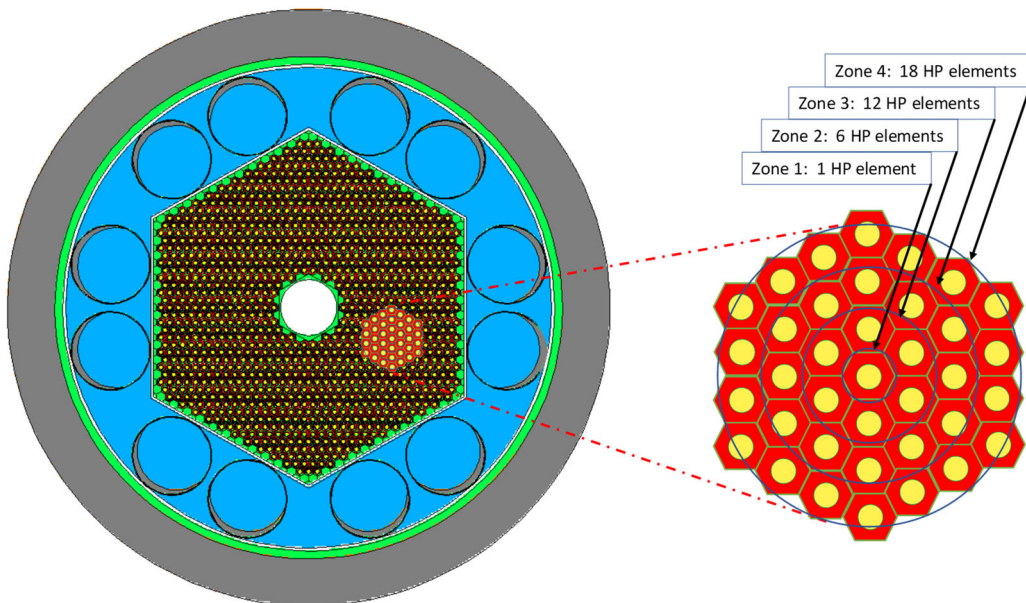


Figure 2-4 Example of cascading HP nodalization.

2.2. MELCOR HPR Failure Models

The MELCOR HP model includes several failure modes. For example, the vapor flow to the condenser is limited by the sonic limit, and the liquid flow returning to the evaporator section is limited by the capillary limit. The three most important failure modes for the HPR demonstration calculations were the boiling limit, HP wall failure due to melting, and HP wall failure due to creep rupture. Each of these failure modes will be discussed next.

The boiling limit is implemented as a maximum local heat flux in a COR cell. The boiling limit is converted to a maximum flux, which is compared to the local COR cell heat flux. If the predicted local COR cell heat flux exceeds the maximum flux, then the heat transfer coefficient between the working fluid and the heat pipe wall is degraded, reflecting inconsistent fluid contact. The boiling limit does not directly fail the HP but will lead to a rapid rise in the local heat pipe wall temperature.

The second mode of HP failure, which follows the boiling limit in the HPR demonstration calculation, is the melting failure of the HP wall. The INL Design A HP uses a stainless steel cladding around the fuel and a stainless steel HP wall. The MELCOR model for the INL Design A HPR assumes the fuel cladding and the HP wall fail simultaneously at 1650 K, which is just below the melting temperature of stainless steel. The heat pipe is at high pressure and temperature and expected to yield as the adjacent fuel cladding temperature approaches the stainless steel melting point. When the HP wall fails, the high pressure fluid exits from the HP and it ceases to operate.

A third failure mode is creep rupture of the HP wall, which could occur well below the stainless steel melting point. As the energy transferred by the HP increases, the operating pressure and temperature of the fluid in the HP increases. As shown in Figure 2-5, the HP pressure rises above atmospheric pressure as the HP fluid temperature increases above approximately 800°C.² At high pressures and temperatures, the HP wall will strain and fail. A creep rupture failure at the top of the core or in the condenser is evaluated using the built-in Larson-Miller lifetime failure model for stainless steel pipes [3]. If the creep rupture criteria are exceeded, then the wall of the HP fails. Similar to the local melting failure in the core, the high-pressure fluid exits from the HP and the HP ceases to operate.

Figure 2-6 shows the HP and the fuel cladding failure locations described above. The fuel cladding failures are particularly important because this begins the start of the fission product release from the fuel. The upper two HP failures are illustrative of creep ruptures at high pressure and temperature. Since the fluid in the HP is approximately isothermal (also an assumption in the MELCOR HP model), a creep failure can occur almost anywhere along the HP wall. However, it should be noted that the pipe wall stress in the condenser is different than the core due to different external pressures on the pipe wall. Weld and flaw locations could be vulnerable but are also difficult to characterize. Once the pipe fails and depressurizes, an additional creep rupture failure is not possible.

² The pressure versus temperature curve in Figure 2-5 is dependent on the HP geometry and the associated fluid mass.

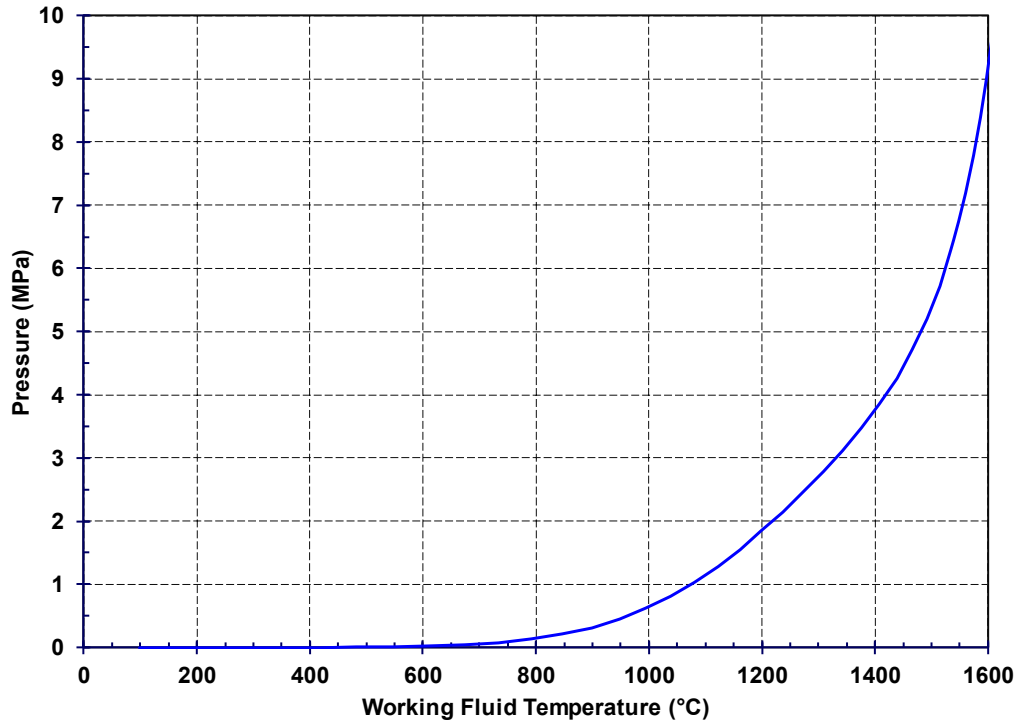


Figure 2-5 Potassium Equilibrium Pressure Temperature Curve.

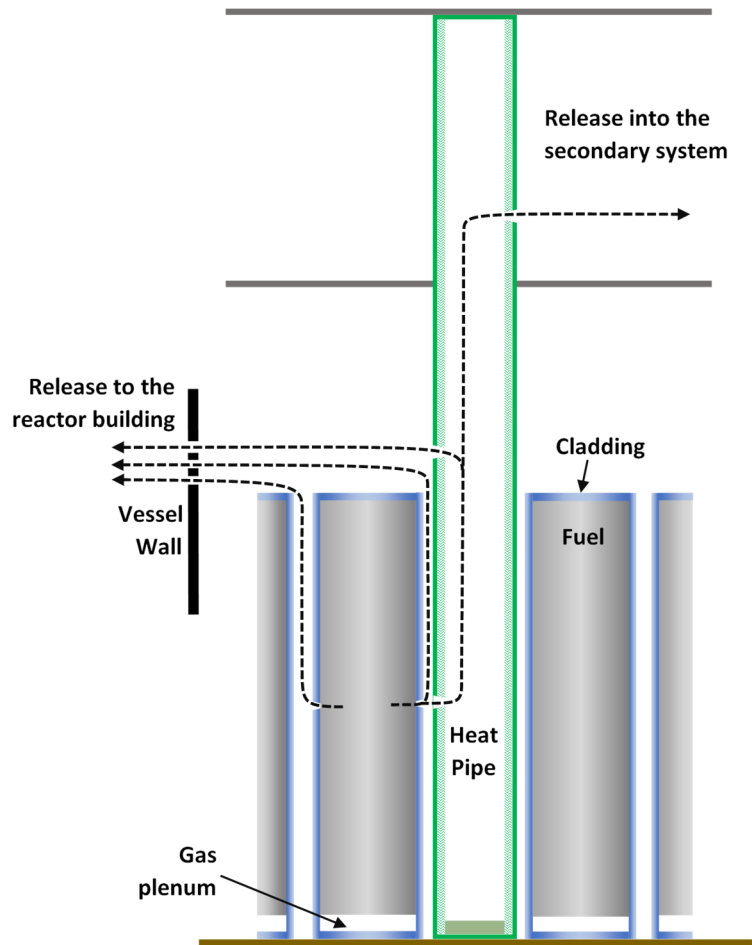


Figure 2-6 HP failure pathways.

3. MODEL DESCRIPTION

The vessel and core of the INL Design A heat pipe model was constructed using information primarily documented in the INL design report [5]. The report provided details for most of the required core and HP input. The HP system performance limits were developed using the LANL HTPIPE code [9], which allows specification of the specific geometry of the INL Design A HP. The INL design report did not include information on the secondary system, which was supplemented using other INL conference presentation material [12]. The LANL and INL design reports did not include information about the surrounding reactor building. The inputs for the reactor building were estimated based on experience with the boiling water reactor (BWR) enclosure building. The radionuclide inventory and decay heat were obtained from a supporting SCALE analysis by ORNL [15]. ORNL also provided the axial and radial power profiles and reactivity feedbacks.

3.1. INL Design A HPR Overview

A cross-section of the INL Design A reactor vessel is shown in Figure 3-1, and the reactor vessel and secondary system schematic are shown in Figure 3-2. The key design features are summarized in Table 3-1. The core is formed in a hexagonal shape with a circular center for the emergency control rods. 1134 hexagonal fuel elements are arranged around the hexagonal core. The core is surrounded by a large (i.e., 19.4-27.3 cm thick) alumina reflector that contains 12 control drums for reactivity control. The control drums can slowly turn the B₄C arcs to increase or decrease reactivity. The alumina reflector is surrounded by a 5.1 cm stainless steel core barrel assembly and a 15.2 cm B₄C radiation shield. There are beryllium oxide reflectors above and below the core.

The active fuel region is 150 cm. The fuel is 19.75 wt% HALEU with a maximum burn-up of 2 GWD/MTU. The mass of the ²³⁵U is 904 kg. The expected design life is 5 years. The demonstration analysis assumed the core burnup was at the end of the cycle, or the expected design life of 5 years.

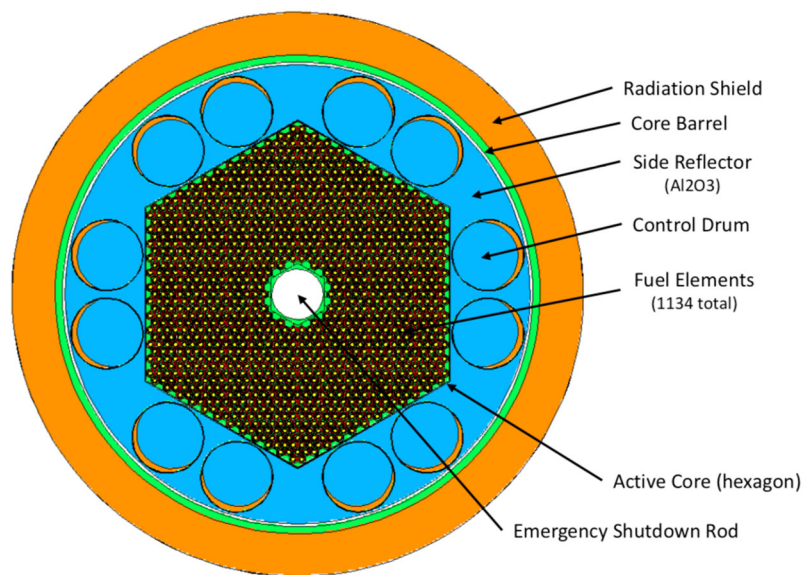


Figure 3-1 INL Design A reactor vessel cross-section [5].

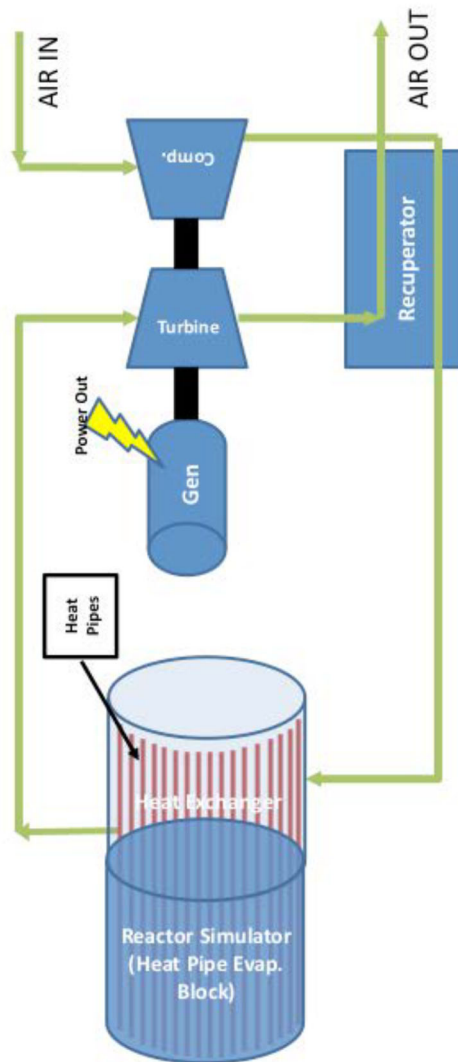


Figure 3-2 INL Design A reactor and secondary design schematic [12].

A cross-section of the INL Design A HP fuel element is shown in Figure 3-3. The circular heat pipe is located in the center of each fuel element. There are very small gaps (0.0064 cm) between HP and the fuel element stainless steel cladding. There are also small gaps between the hexagonal fuel element and the inner and outer cladding. The fuel element pitch is 2.7862 cm. The HP outer diameter is 1.757 cm with a 0.1 cm wall thickness. The heat pipe is 4 m long with a 1.5 m segment in the condenser region. The adiabatic length is 0.4 m. The average heat pipe power is 4.41 kW.

The performance limit curves for input into MELCOR were generated using the LANL HTPPIPE code [9]. The INL Design A geometry and the selection of a potassium working fluid were provided to HTPPIPE. The curves generated by HTPPIPE are shown in Figure 3-4.

Table 3-1 Key Parameters for the INL Design A HPR [5].

Parameter	Value
Reactor thermal power	5 MW
Fuel elements	1134 hex elements 5.2 MT of UO ₂ 19.75 wt% enrichment
HPs	1134 HPs with potassium working fluid
Reactivity control	12 alumina control drums with arcs of B ₄ C for reactivity control
Shutdown system	2 B ₄ C emergency control rods
Secondary system	Brayton open-air power cycle

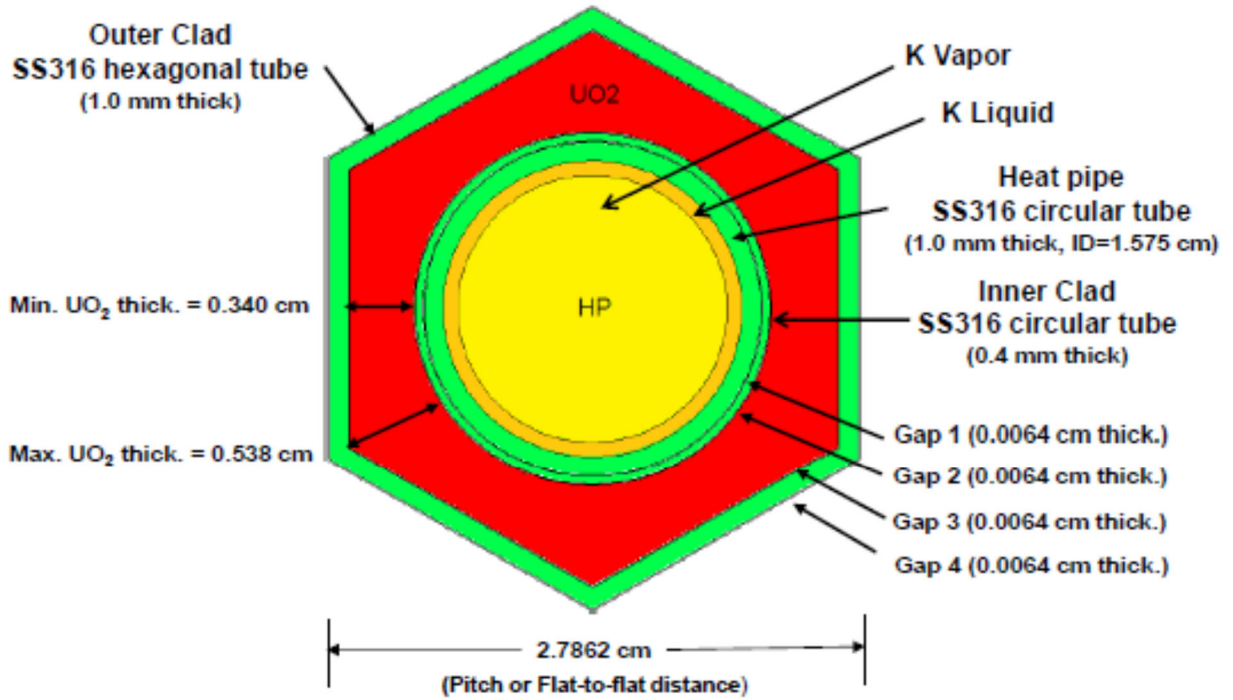


Figure 3-3 INL Design A HP and fuel element cross-section [5].

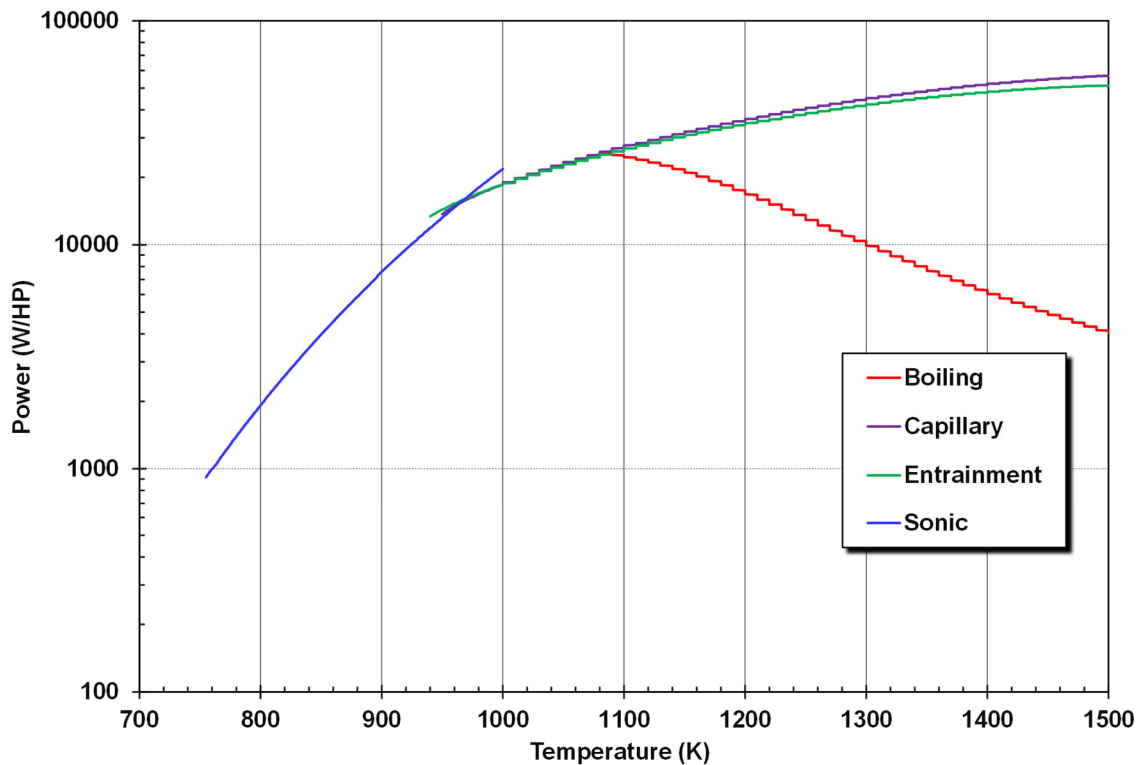


Figure 3-4 HP limit curves for the INL Design A MELCOR model using HTPIPE.

3.2. Reactor Vessel Nodalization

The modeling of the INL Design A reactor vessel in MELCOR utilizes building block inputs from multiple packages. The building block approach to the input gives lots of flexibility to model alternative reactor designs with varying levels of resolution. A key set of vessel input comes from the COR Package, which includes the structures in the core and the radionuclide release model. The INL Design A COR nodalization has 14 axial levels and 15 radial rings, which are in cylindrical coordinates (see Figure 3-5). The COR package includes (a) the active core region with the evaporation section of the HPs (i.e., the region within axial levels 3-12 and rings 2-15), (b) the center, top and bottom reflectors surrounding the core, (c) the HP extension through the adiabatic region (axial level 13) and the condenser region (axial level 14), (d) the outer baffle plate surrounding the hexagonal core (also in ring 15), and (e) the region below the active core that includes bottom reflector and the fuel gas plenum in axial levels 1-2. The large alumina side reflectors, the core barrel, and the B₄C radiation shield are modeled in the heat structure (HS) package but are thermally coupled to the COR region (see Figure 3-1). There is equal spacing between the radial rings in the active core (rings 2-15) that corresponds to the width of a fuel element (28 cm). There are 10 equally spaced (15 cm) axial levels in the active core.

Each COR ring includes a separate HP model that corresponds to the number of HPs within the ring radii. The HPs are assumed to respond identically within a COR ring. However, MELCOR includes the flexibility to have HPs with alternate characteristics (e.g., the limit or failure criteria) within the same ring. Each HP becomes a normal fluid control volume (CV) upon its failure (i.e., CV-251 through CV-264). The CVs track the pressure and temperature in the HP and

depressurize into the vessel or the secondary side upon their failure. There are provisions for a heat pipe wall melting failure and creep failures in the vessel and condenser regions for each of the 14 rings with HPs in the core. The failures are modeled with flow paths connected to the appropriate failure signals.

A single control volume is used to represent the interstitial regions around the fuel elements (i.e., CV-200, see Figure 3-6). CV-400 represents the secondary side of the condenser with flow path connections for the upstream and downstream secondary boundary conditions. The secondary is assumed to blowdown to the atmosphere when the secondary recirculation fan trips off. The interstitial regions in lower plenum are modeled with CV-100. There are variable sized leakage paths from the lower plenum and adiabatic regions to the reactor building where released radionuclides can leak out (see FL-400 and FL-405 on Figure 2-6, respectively). An uncertainty study examined the importance of the vessel leakage area on the system response and the magnitude of the source term, which was reported in the public presentation [7].

The COR package also includes the heat transfer and physics routines for the materials in the core, any material relocation, the eutectic interactions, the support structure degradation, and the lower reactor head heatup and failure. The demonstration calculations included melting and relocation of some stainless steel cladding material but the predicted conditions were not severe enough to result in gross relocation of the fuel elements.

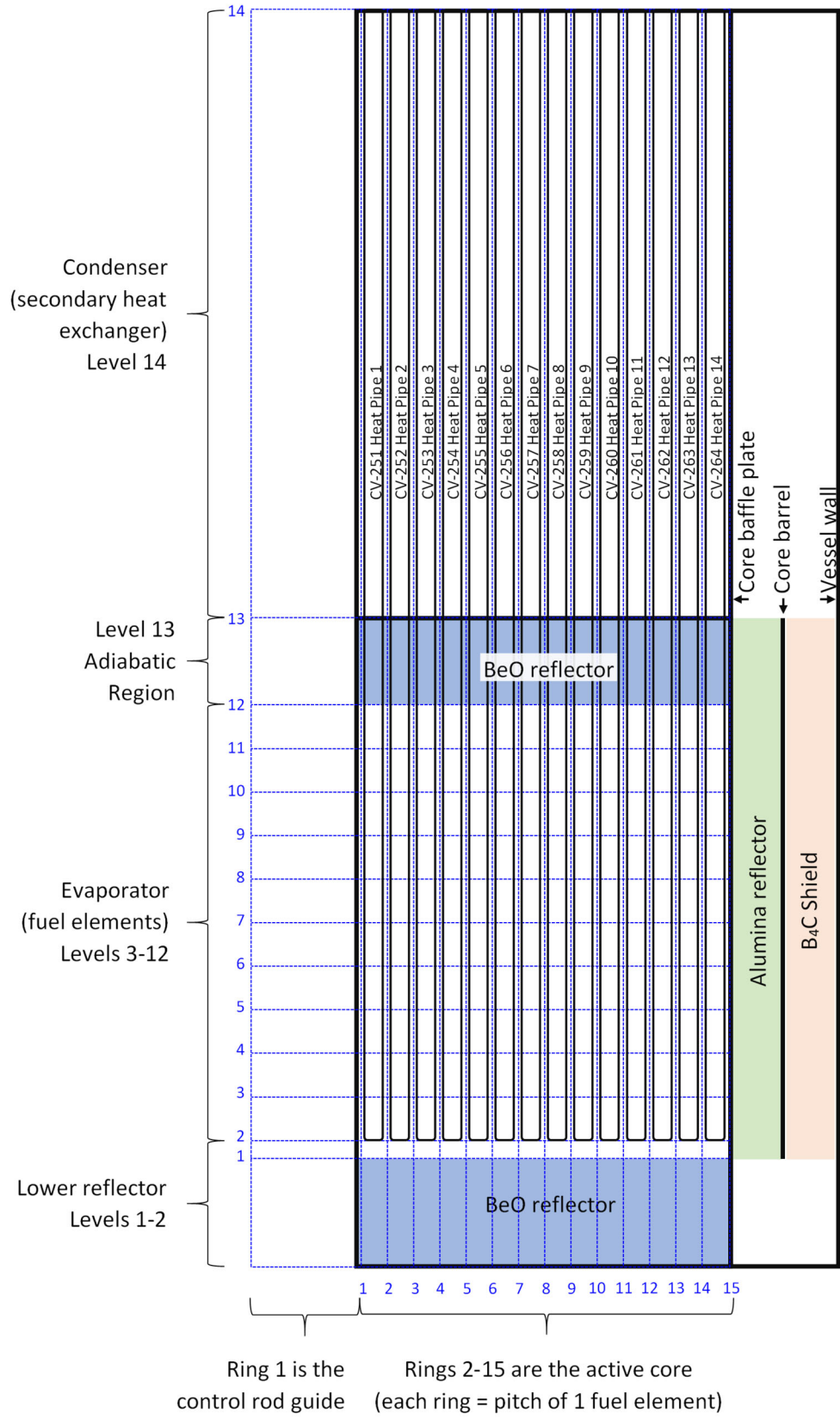


Figure 3-5 INL Design A reactor vessel HP nodalization.

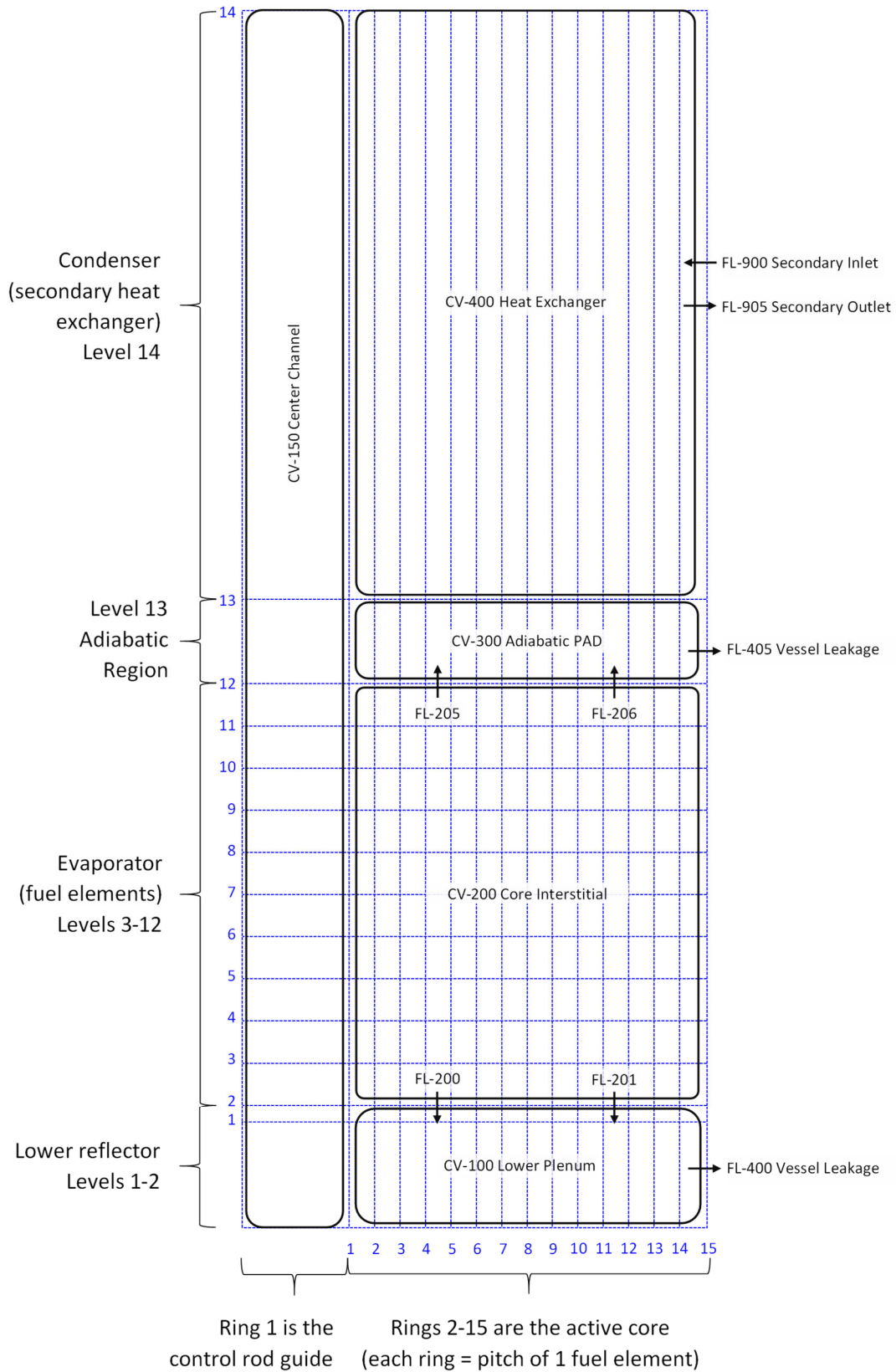


Figure 3-6 INL Design A reactor vessel volume and flow path nodalization.

3.3. Reactor Building Nodalization

A reactor building model was developed based on the concept of the BWR reactor building surrounding a BWR/4 Mark I containment. The INL Design A report indicated that the reactor should be placed in a concrete reactor cavity for additional shielding protection. It was assumed that the reactor would be below-grade with a surrounding building that includes below-grade and above-grade rooms, as shown in Figure 3-7. The first floor around the reactor would have limited access. The turbine, compressor, and recuperator are located on the second floor (see Figure 3-2).

The reactor cavity, the first floor, and the second floor were modeled with separate CVs. There are two flow paths between each region to facilitate natural circulation. The reactor cavity flow areas were estimated based on the open space between the vessel and cavity wall. The flow paths between the first and second floor of the reactor building are modeled as the area of two stairwells.

The building leakage was scaled similar to a BWR reactor building (i.e., 100% leakage per day at a design pressure of 0.25 psi). When there is an external wind, one flow path is assigned to the upwind side of the building and the other is on the downwind side. The guidance for modeling wind effects on leakage from a building is described in Reference [13]. External wind effects are included in DOE facility safety analysis where there are not strong internal building driving forces for radionuclide release. The wind increases the building infiltration and exfiltration rates. The upwind infiltration location was modeled using FL-5025 and the downwind location was modeled using FL-5010 when an external wind was considered. The wind effects are modeled as an additional Bernoulli pressure term in the flow path pressure solution,

$$dP_{Wind} = \frac{1}{2} \rho C_p v^2$$

where,

dP_{Wind}	Bernoulli wind pressure term, (Pa)
ρ	Fluid density, (kg/m ³)
C_p	Building coefficient, (-)
v	Wind velocity, (m/s)

The values for the building coefficients are typically obtained using computational fluid dynamics evaluations. When wind effects are modeled in the demonstration calculations, generic building coefficients were obtained from the American Society of Heating, Refrigerating and Air-Conditioning Engineers (ASHRAE) handbook (see Table 3-2 [14]).

Table 3-2 Typical building coefficients [14].

Wind Direction	Value
Upwind	0.7
Downwind	-0.4
Side and top of the building	-0.35

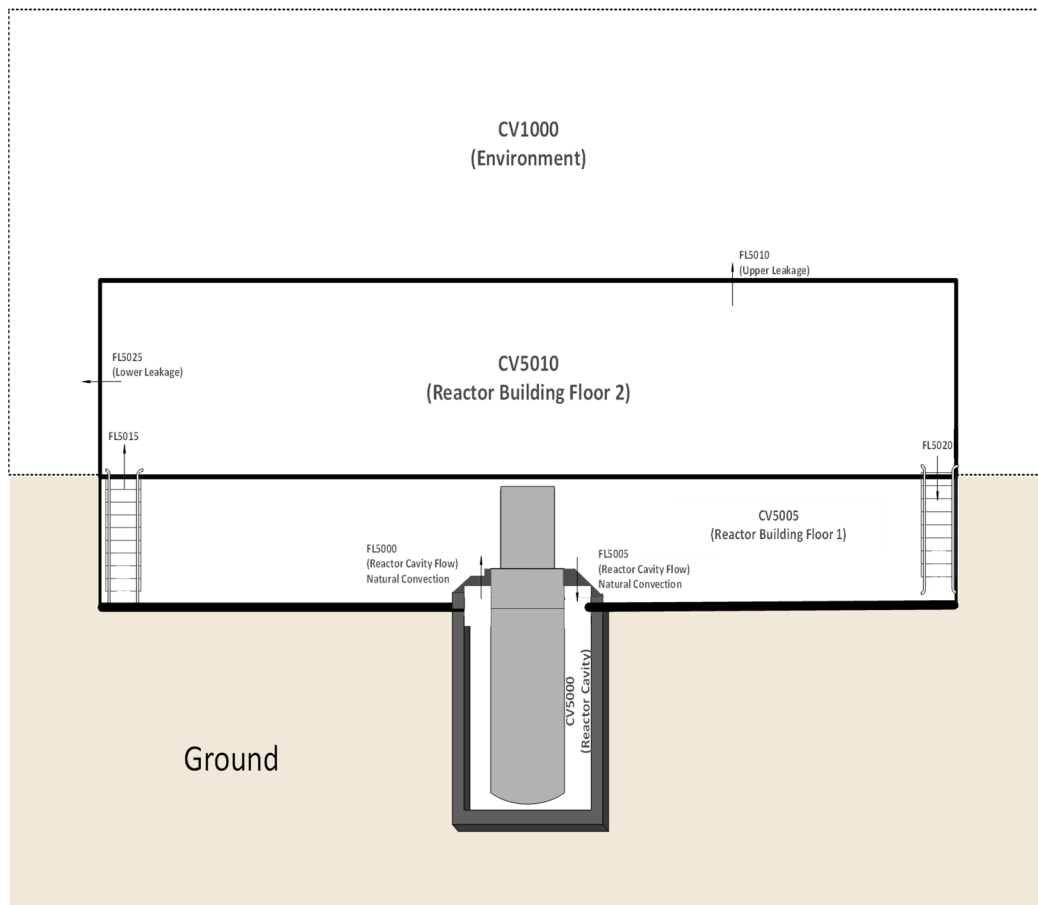


Figure 3-7 HPR reactor building nodalization.

3.4. Radionuclide Inventory

The INL Design A radionuclide inventory and decay heat input were calculated using SCALE by ORNL [15]. The radionuclides from the SCALE calculations were grouped and assigned to one of the twelve MELCOR radionuclide classes. The 5-year end-of-cycle burn-up results were used for the demonstration calculations, which was approximately 2 GWd/MTU. The data provided from SCALE includes separate decay heat curves for each of MELCOR's radionuclide (RN) classes. The overall decay heat is shown in Figure 3-8.

The axial and radial power profiles were also provided by ORNL using SCALE [15]. The axial profile is approximately cosine-shaped with a maximum axial peaking factor of 1.25. The top and bottom of the axial power profile have strong peaks (i.e., 1.04 at the bottom and 0.79 at the top) due to the proximity the top and bottom beryllium reflectors, respectively (see Figure 3-9). The radial power is skewed toward the center with a maximum of 1.4 at the fuel elements closest to the center (see Figure 3-10). Due to the very low burn-up of the INL Design A reactor, there was very little difference between the beginning of the cycle (i.e., 3 days (0.008 years) in Figure 3-9 and Figure 3-10) versus the end-of-cycle profile (i.e., 5 years).

The radionuclide inventory from SCALE is collapsed into MELCOR's 12 RN classes as shown in Table 3-3. Table 3-4 shows the radionuclide class inventories provided by SCALE. The results were further subdivided to include compounds of cesium iodide and cesium molybdate (e.g., see

Reference [16]). Variable gaseous iodine amounts were explored that spanned from 0% to 5% of the iodine inventory. The remaining iodine was assumed to bond with cesium to form cesium iodide. The remaining cesium was subdivided as 20% cesium iodide and 80% cesium molybdate. The cesium and iodine speciations have uncertainties and are often treated as uncertain parameters (e.g., References [17][18][19]). In the accidents simulated in this report, the temperatures in the HPR core were relatively low after the volatile radionuclides were released. Due to these relatively low temperatures, the differences in the various compound vapor pressures are not expected to be as significant as in light-water-reactor accidents (e.g., an unmitigated station blackout in boiling water reactors, see Reference [20]). The HPR public workshop for this project included examples of uncertainty sampling of iodine gas fraction [7].

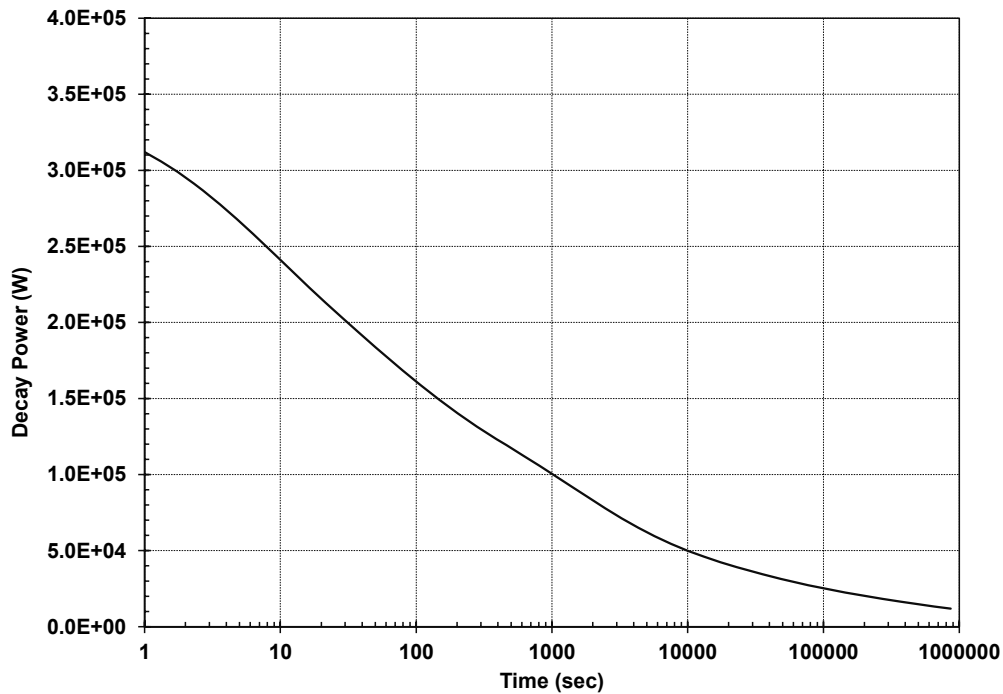


Figure 3-8 HPR decay heat power.

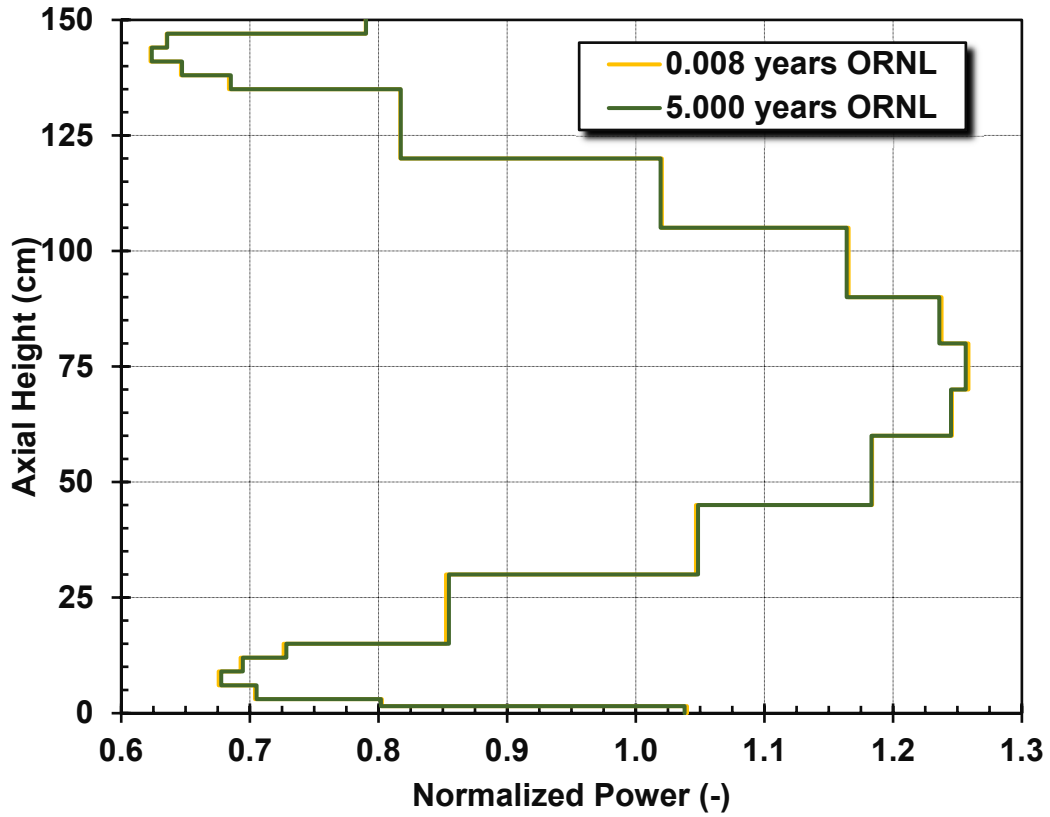


Figure 3-9 HPR axial power profile at the beginning and end of the fuel cycle [7].

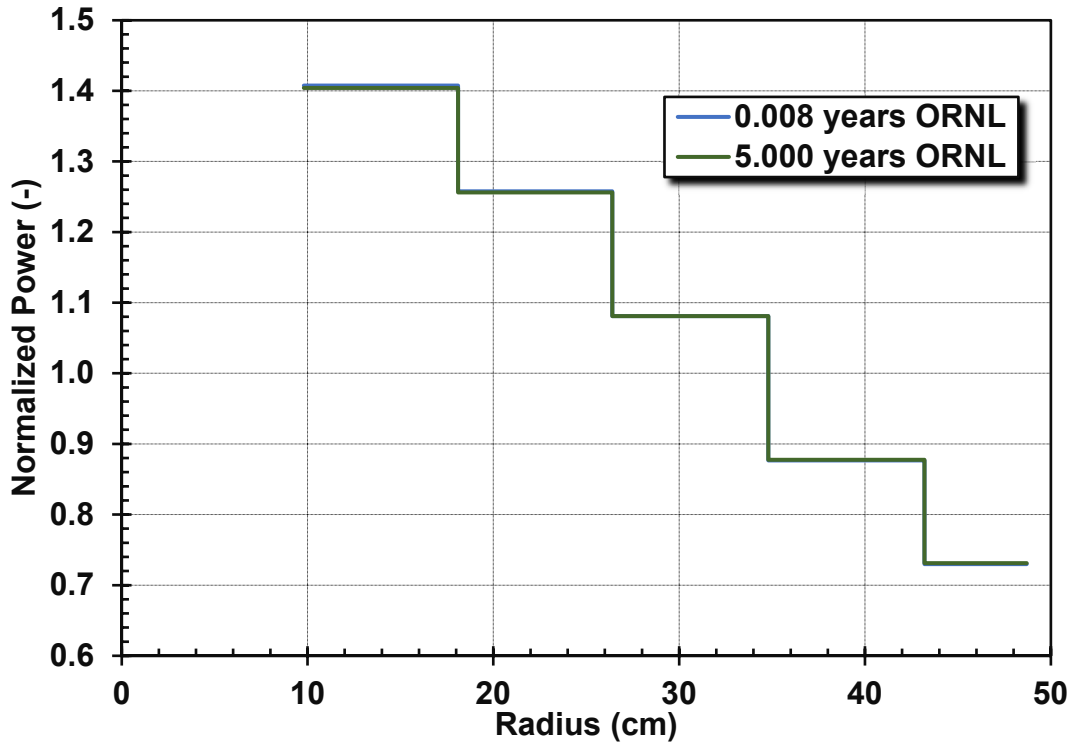


Figure 3-10 HPR radial power profile at the beginning and end of the fuel cycle [7].

Table 3-3 MELCOR radionuclide classes

Class	Class Name	Chemical Group	Representative	Member Elements
1	XE	Noble Gas	Xe	He, Ne, Ar, Kr, Xe, Rn, H, N
2	CS	Alkali Metals	Cs	Li, Na, K, Rb, Cs, Fr, Cu
3	BA	Alkaline Earths	Ba	Be, Mg, Ca, Sr, Ba, Ra, Es, Fm
4	I2	Halogens	I ₂	F, Cl, Br, I, At
5	TE	Chalcogens	Te	O, S, Se, Te, Po
6	RU	Platinoids	Ru	Ru, Rh, Pd, Re, Os, Ir, Pt, Au, Ni
7	MO	Early Transition Elements	Mo	V, Cr, Fe, Co, Mn, Nb, Mo, Tc, Ta, W
8	CE	Tetravalent	Ce	Ti, Zr, Hf, Ce, Th, Pa, Np, Pu, C
9	LA	Trivalentes	La	Al, Sc, Y, La, Ac, Pr, Nd, Pm, Sm, Eu, Gd, Tb, Dy, Ho, Er, Tm, Yb, Lu, Am, Cm, Bk, Cf
10	UO ₂	Uranium	UO ₂	U
11	CD	More Volatile Main Group	Cd	Cd, Hg, Zn, As, Sb, Pb, Tl, Bi
12	AG	Less Volatile Main Group	Ag	Ga, Ge, In, Sn, Ag

Table 3-4 HPR radionuclide class masses.

MELCOR RN class	MELCOR Class Mass (kg)
Noble Gases (Xe)	1.323E+00
Alkali Metals (Cs)	1.184E+00
Alkaline Earths (Ba)	7.211E-01
Halogens (I)	5.265E-02
Chalcogens (Te)	1.383E-01
Platinoids (Ru)	7.598E-01
Early Transition Elements (Mo)	1.226E+00
Tetravalent (Ce)	6.755E+00
Trivalentes (La)	2.287E+00
Uranium (U)	4.561E+03
More Volatile Main Group (Cd)	1.083E-02
Less Volatile Main Group (Ag)	1.697E-02

3.5. Radionuclide Release Input

The MELCOR fuel release model calculates the release of radionuclides from the fuel elements. MELCOR's CORSOR-Booth model, which has been benchmarked to available LWR fuel release data for UO₂ ceramic fuel [21], was used to predict the radionuclide release. The low-burnup option of the CORSOR-Booth model was selected for the HPR. The magnitude of the radionuclide release is a strong function of the time at high temperatures. As a surrogate for uncertainties in the radionuclide release model, the uncertainty assessment presented at the HPR public workshop for this project included uncertain parameter specifications to vary the peak fuel temperature and the core heat removal, which led to variations in the radionuclide release from the fuel [7].

3.6. Point Kinetics Modeling

MELCOR includes a fast-running, six-group point kinetics model for the dynamic simulation of the reactor power. The INL Design A reactivity feedbacks were calculated by ORNL from their full-core, 3-dimensional, continuous energy simulations. The ORNL predictions were in good agreement with the INL design report. The ORNL analysis included the radial expansion effects of the stainless steel clad, the gap closure and changes in the fuel pitch, the alumina radial expansion, and the control drum drift. The ORNL-predicted feedback coefficients are shown in Table 3-5.

Table 3-5 INL Design A reactivity feedback coefficients [15].

Feedback Effect (cents/°C)	SCALE
Doppler	-0.1113
UO ₂ Fuel Axial Elongation	-0.0437
Alumina Reflector Radial Thermal Expansion	-0.0284
All Radial Expansions (Clad, Reflector, and CDs)	-0.0636
Total	-0.2185

The reactivity feedbacks shown in Table 3-5 illustrate important inherent safety features of the INL Design A HPR. The system has a very strong negative reactivity response to a temperature rise. Consequently, the reactor fission reaction will naturally shut down as the temperature rises in an overheating accident due to fuel Doppler and expansion effects. Conversely, the reactivity will increase as the reactor cools, which provides a degree of inherent control during normal operations. The operators (or the control system) will make small adjustments to the control drum rotational position for normal power operations.

ORNL predicted the total drum worth was \$11.38, which agreed well with Reference [5]. The total drum reactivity was used to determine the relationship between the reactivity insertion rate and the control drum rotation speed. ORNL also provided the annular and solid emergency control rod worth (i.e., \$11.75 and \$9.70, respectively). It was assumed that both control rods inserted over 10 seconds when the reactor protection system was actuated.

4. EXAMPLE RESULTS

The INL Design A input model was used to demonstrate MELCOR's HPR MST capabilities. A TOP scenario was chosen to be the focus of this demonstration after reviewing the results from MELCOR simulations for the TOP, loss-of-sink accident (LOHS), and ATWS scenarios. The TOP scenario generated a source term whereas the latter two scenarios did not. The results from variations in some of the key reactor building performance parameters are also presented. Additional results from a Monte Carlo uncertainty analysis were shown in the public workshop but not discussed here [7]. The base and sensitivity TOP scenario results are discussed in Sections 4.1 and 4.2, respectively. The discussion of the calculations includes the thermal-hydraulic response of the reactor and the associated radionuclide release behavior. Example LOHS and ATWS scenario results are discussed in Section 4.3 that did not have a radionuclide release. MELCOR Version 19513 was used for the HPR analysis.

Another accident scenario of potential concern for heat pipe reactors is the failure of one or more heat pipes, which may lead to cascade failure. A "cascade failure" is the loss of a single or multiple heat pipes that causes the failure of surrounding heat pipes in a cascade. If enough heat pipes fail, the reactor core may overheat [6]. While a cascade failure scenario was not analyzed for this project, it could be simulated with MELCOR using an alternate nodalization of the core (i.e., see the discussion in Section 3.2).

4.1. Transient Overpower Scenario

The TOP scenario is initiated with a spurious rotation of the control drums such that the B₄C arcs turn away from the reactor core. The rotation of the control drums causes an increase in the core reactivity. A maximum rotation speed was selected that would provide dynamic control during start-up and normal operations but a degree of safety from rapid changes.

ORNL calculated the drum reactivity worth as a function of rotation angle. The analysis predicted a 65 degree rotation from the $k_{\text{eff}}=1$ drum position to a rotational angle with a \$4.021 excess reactivity. Using this information, a rotation speed of 0.0016 deg/s was specified to yield a reactivity insertion rate of 1×10^{-4} \$/s. The assumed drum rotational speed and reactivity insertion rate caused the core power to approximately double over 1 hr. However, the uncertainty study explored the impact of increasing and decreasing the reactivity insertion rate by up to an order of magnitude [7].

The safety controls of the INL Design A were not described. A complete HPR design would have a reactor protection system for the automatic emergency control rod insertion. The plant automatic emergency control rod shutdown system is assumed to not operate in the TOP scenario. However, the operators recognize the event and manually insert the controls rods after a time delay. The manual operation action was delayed until after the start of the fuel cladding failures (e.g., after high radiation signals). The scenario also assumes the trip of the secondary circulation system at the time of the manual SCRAM. Consequently, there is no active heat removal after the manual SCRAM.

4.1.1. TOP Reactor Response

The TOP reactor power response is shown Figure 5. After an accelerated steady state calculation to establish the reactor reflector and radiation shield structure's long-term temperature profile, the transient starts with a spurious rotation of the control drums. The increase in core reactivity leads to a power increase and a corresponding fuel and HP heat-up. Due to the very strong negative core reactivity with temperature, the increase in control drum reactivity is matched with a corresponding negative temperature reactivity feedback as the system power and temperature increase. The control

drum reactivity addition and negative temperature feedback somewhat balance to yield a nearly linear power increase but with an associated fuel and HP temperature rise.

As indicated on Figure 4-1, the power increases from 5 MW to 8 MW over the first 0.9 hours. At 0.9 hours into the accident, the core ring with the highest power reaches the boiling limit. The core power drops due to the additional negative feedback as portions of the core rapidly increase in temperature. The manual emergency control rod insertion is assumed to occur just after 1 hour.

The maximum fuel temperature response in Figure 4-2 illustrates the linear temperature rise prior to reaching the boiling limit. The maximum fuel temperature location gradually heat-ups to 1300 K ($\sim 1025^{\circ}\text{C}$). However, once the boiling limit is reached, the heat transfer to the HP fluid degrades at that location and there is a rapid local heatup of the fuel (i.e., similar to a transition from nucleate boiling to film boiling in a water system above the critical heat flux). The cladding melts as the fuel passes the melting temperature of the stainless steel cladding, which starts the radionuclide release from the fuel. The affected HPs are assumed to fail and depressurize, which ends the HP heat removal along the full length of the affected fuel element.

The manual emergency control rod insertion occurs just after 1 hour, which terminates the fission reaction. The secondary system is assumed to trip off at the same time, which stops all active heat removal. The termination of the fission reaction is followed by a strong passive heat dissipation away from the highest fuel temperature location. The fuel cooldown pauses near 1700 K as molten stainless steel refreezes. The heat from the highest temperature regions near the center of the core steadily flows outward to the large surrounding reflector and radiation shield. As the outer vessel heats, a natural circulation of heated air leaves the reactor cavity to the first-floor region and is replaced by cooler air. The passive heat dissipation from the highest temperature fuel locations outward and the subsequent natural convection heat removal from the reactor vessel to the cavity reduces the peak fuel temperature from 2200 K to 1200 K by 24 hours.

The response of the peak fuel temperature can be shown on the HP performance limit graph (see Figure 4-3). As the HP power increases from the control drum reactivity insertion, the HP temperature increases. Once the HP reaches the boiling limit, the wall heat transfer decreases, which causes a rapid increase in the fuel temperature. The fuel cladding and HP wall are predicted to fail when the fuel reaches 1650 K. The trajectory of the power and temperature response on Figure 4-3 is a function of the secondary heat removal characteristics due to the close coupling between the fuel, the HP fluid temperature, and the HP wall temperature in the secondary condenser. As shown on the figure, only the boiling limit would be challenged in this scenario.

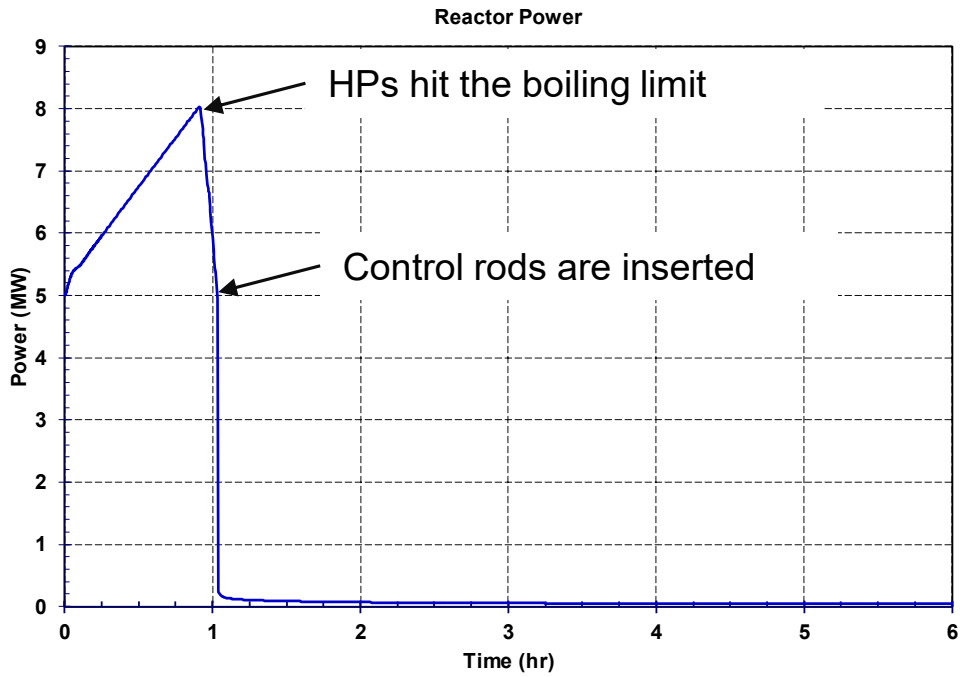


Figure 4-1 Reactor power response in the TOP scenario.

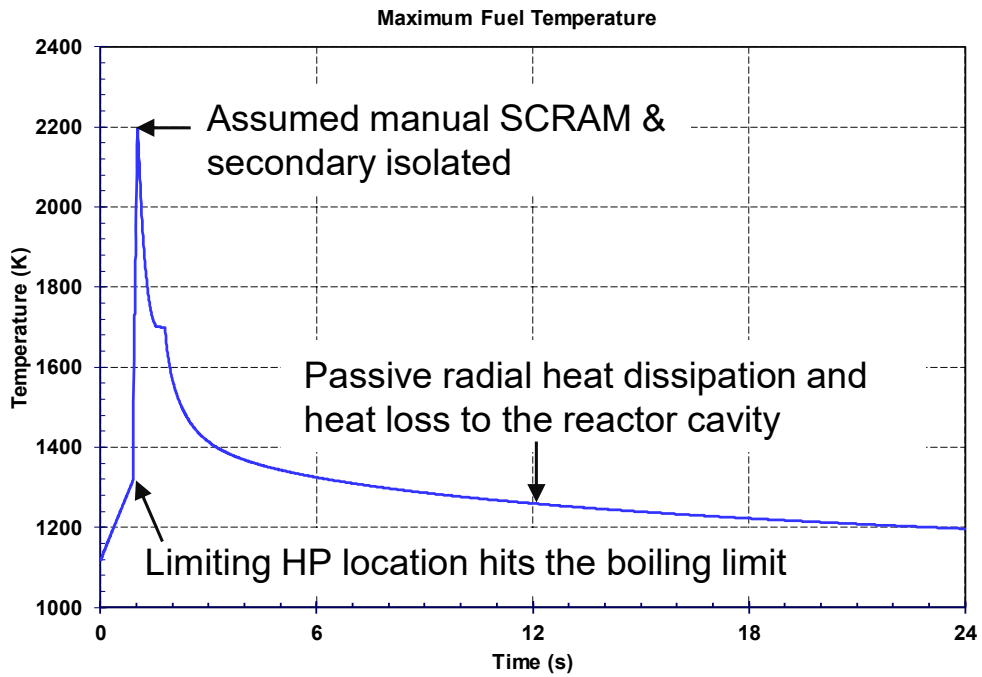


Figure 4-2 Maximum fuel temperature response in the TOP scenario.

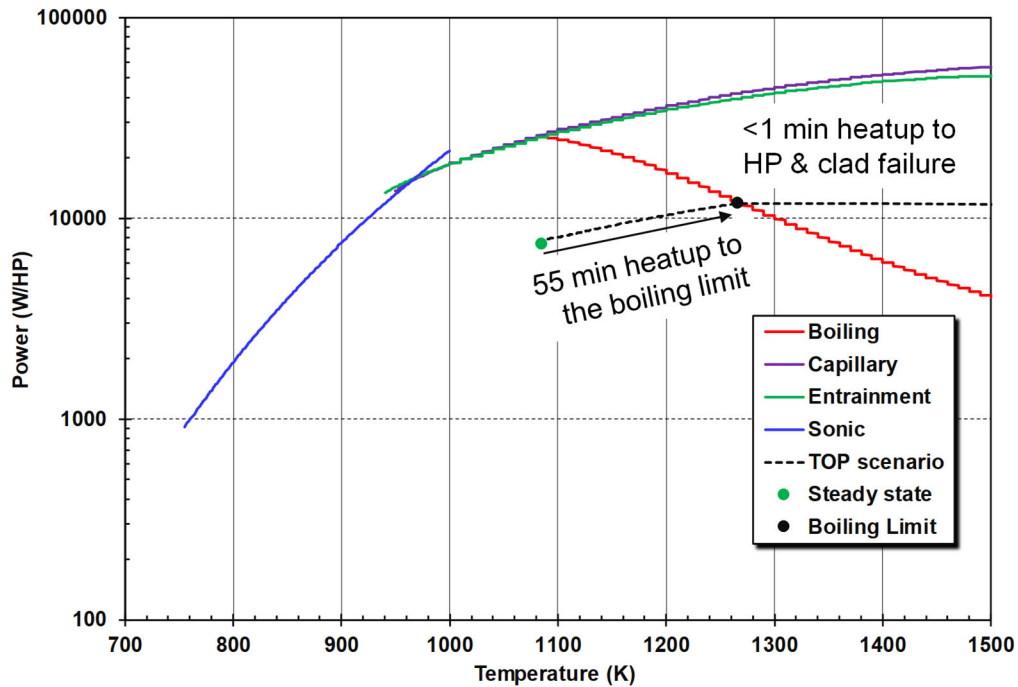


Figure 4-3 TOP scenario response on the HP performance limit graph.

4.1.2. TOP Radionuclide Response

The pressure response of the heat pipes is shown in Figure 4-4. Approximately 20% of the 1134 HPs failed (i.e., the ones at atmospheric pressure after their failure). The failures occurred in the 6 inner rings of the MELCOR core nodalization (i.e., Rings 2-7 on Figure 3-6). When the HPs reached the boiling limit at the highest-powered location, the HP pressure and temperature dropped rapidly in response to the sudden reduction in heat addition but with the continued heat removal from the secondary system. Consequently, the HPs failed closer to 2 bar rather than the peak value of up to 6 bar shown in Figure 4-4.

The HP wall failed at the time of the fuel cladding failure (i.e., a modeling assumption), releasing potassium vapor which provided a short-term motive force to push any promptly released fission products out of the reactor vessel. Due to the very low fuel burnup, the initially mobile radionuclide inventory in the gaps around the fuel is expected to be very small. Consequently, the HP blowdown had a relatively small impact on the initial radionuclide release. Furthermore, the relatively low peak temperature (2200 K at the hottest fuel location) was followed by a prompt cooldown (see Figure 4-2). Therefore, the time-at-high temperature for radionuclide release was a relatively short duration.

The iodine release from the fuel and its distribution is shown in Figure 4-5. About 1.4% of the iodine inventory was released from the fuel. The assumed leak area from the vessel was 10.3 cm² (1.6 in²). However, there was relatively little motive force to discharge the iodine from the vessel into the reactor building after the failed HP depressurizations. Furthermore, the release of iodine from the fuel diminished quickly following the reactor cooldown after the emergency control rod insertion. The long-term prediction (i.e., at 24 hr) was 89% of the released iodine remained in the vessel and only 11% in the reactor building or the environment.

The overall iodine release to the environment was 0.0008% of the total iodine fuel inventory. The reactor building leakage to the environment was affected by the small, assumed leak area of 11.6 cm² (1.8 in²), the lack of any significant pressurization of the reactor building, and the dilution and settling in the reactor building prior to reaching the above grade leakage locations.

The active radionuclide release pathways from the cladding failure locations to the vessel leak location are highlighted in red in Figure 4-6. The release pathway in the TOP scenario is through the failed fuel cladding and into the reactor building through leakage locations in the reactor vessel.

It is possible (but was not predicted) in the TOP scenario that the released radionuclides could bypass the reactor building. If there was a creep rupture failure in the HP condenser prior to the HP wall melt-through, then there is a more direct pathway from the core to the secondary side of the condenser. However, even this pathway requires a subsequent HP wall failure in the core to complete the core to secondary pathway. The bypass pathway in an open Brayton cycle discharges directly to the environment if the secondary is not isolated.

Figure 4-7 shows the HP creep failure index. If the creep rupture index reaches 1, then the HP is assumed to fail. The creep index has an exponential increase at high temperatures and pressures that could lead to a creep failure in the HP wall. However, the HPs which failed due to melting at the boiling limit location only reached a maximum of 6 bar prior to their failure and were not at risk of a creep failure. The remaining HPs reached much higher pressures (i.e., up to 13.5 bar) during the cooldown phase after the control rod insertion. For the intact HPs, there was not any danger of a HP melting failure in the evaporator region, and there was no late HP creep failure in the condenser region.

The maximum HP pressure and creep index occurred in the Ring 8, which was adjacent to the last ring with a HP boiling limit transient and wall melt-through. A creep failure after the cooldown is not a risk of a direct pathway to the secondary and the environment because the HP would only have one failure location (i.e., two are needed for a flow pathway). Furthermore, a creep rupture failure cannot occur after a melt-through failure in the core because there is no driving pressure or temperature in the HP to further increase the creep. In summary, the creep index was too low for a creep failure (i.e., $<10^{-6}$) when the boiling limit transient caused a wall melt-through.

Some exploratory calculations showed it is very unlikely to have a HP creep failure prior to a boiling limit melt-through in the TOP scenario. An additional system failure would be required (e.g., the trip of the secondary heat removal system prior to reaching the boiling limit). A secondary heat removal system trip with a sustained reactivity insertion causes a steady increase in the fuel and HP temperatures. If the HP pressurizes and heats to the creep limit in the secondary system before reaching the boiling limit, then one half of the release pathway is created. The HP wall in the evaporator section must subsequently fail to complete the pathway from the core to the secondary. The likelihood of a HP creep failure in this modified scenario is more likely if the control drum rotation rate is slowed and the manual shutdown action is further delayed.

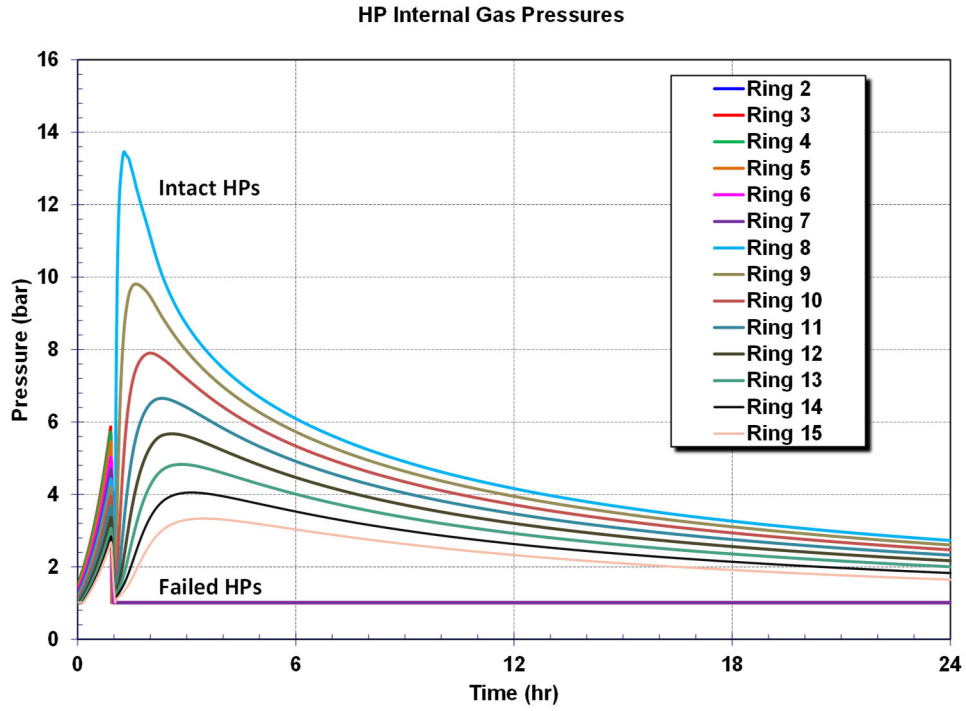


Figure 4-4 The failed and intact HP pressure response in the TOP scenario.

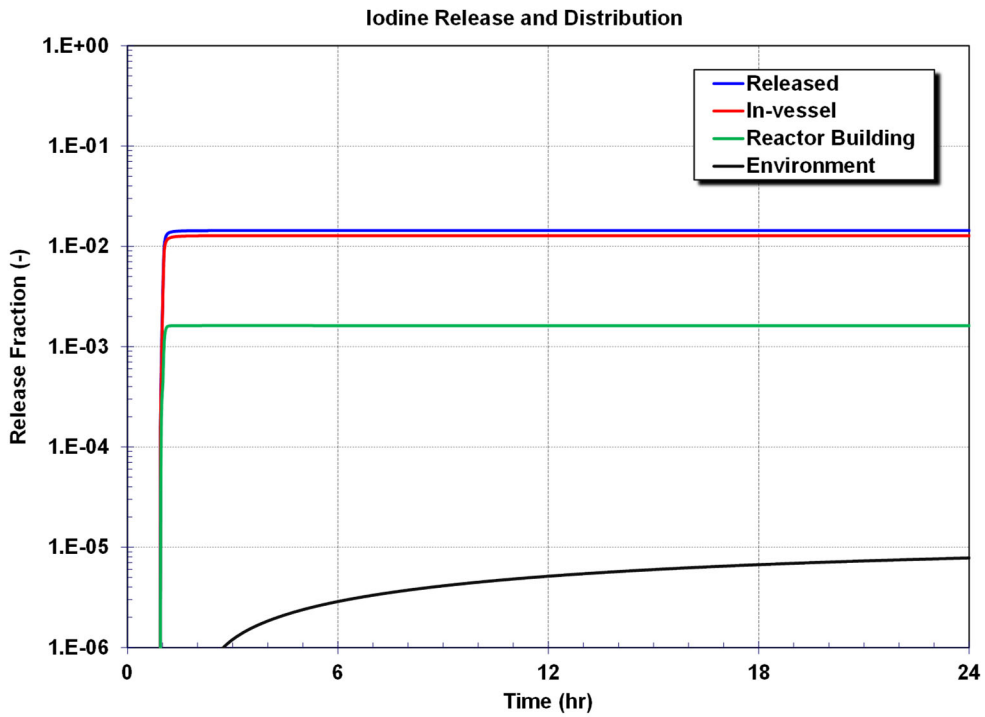


Figure 4-5 Iodine release and distribution in the TOP scenario.

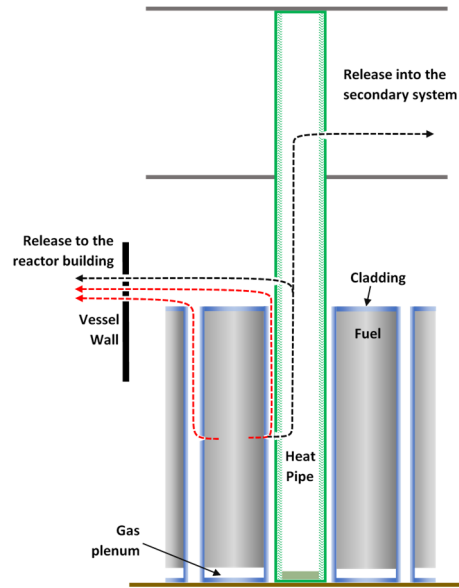


Figure 4-6 Iodine release pathway in the TOP scenario.

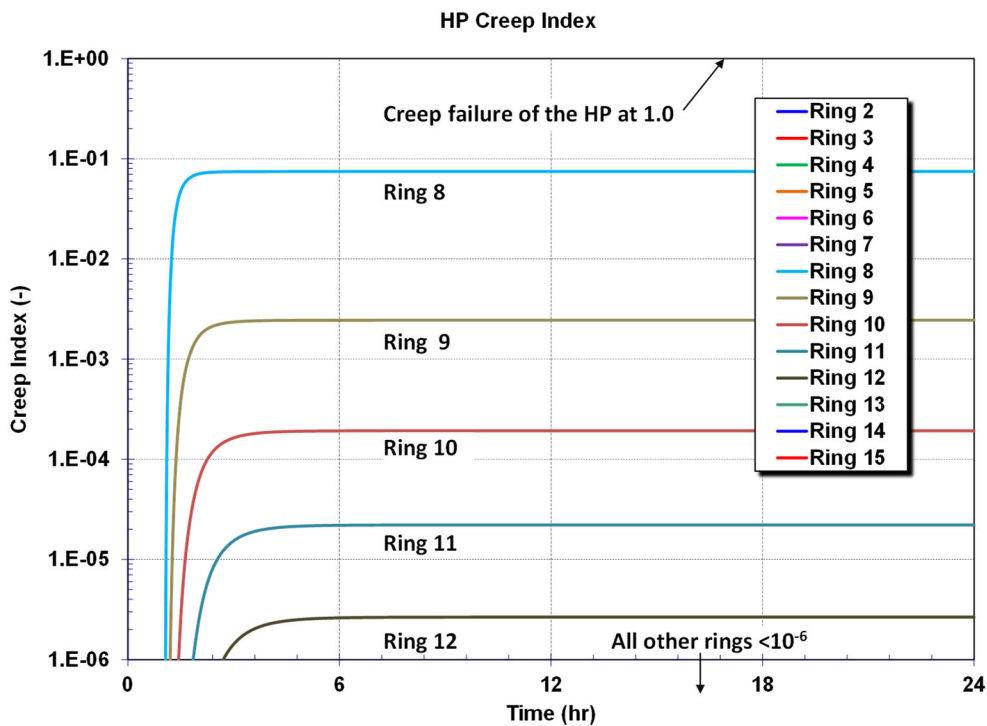


Figure 4-7 HP creep rupture index in the TOP scenario.

4.2. Transient Overpower Scenario Sensitivity Calculations

MELCOR is well-suited for exploring calculational sensitivities. Many parameters in the physics routines can be sampled and varied in sensitivity calculations. In addition, MELCOR's building block format and integrated control logic allows flexible specification of the uncertain or variable boundary condition parameters. A number of uncertain parameters were identified that could impact the accident progression or the magnitude of the source term (see Table 4-1). The parameters in the

table are not intended to be exhaustive or representative of a formal phenomenon identification and ranking table. Instead, the parameters and their ranges were selected for a preliminary investigation of their impact on key figures of merit, as well as a demonstration of the ability to explore their importance in the source term prediction. The following examples varied one parameter at a time at their maximum and minimum. However, the next logical application is a Monte Carlo uncertainty sampling of all uncertain parameters simultaneously. An example of a Monte Carlo uncertainty analysis was provided in the public workshop slides [7].

As an example of single variations of uncertain parameters, the reactor building leakage rate and the external wind speed were selected. Figure 4-8 shows the iodine release to the environment with variations in the building nominal leakage rate and the external wind speed. As discussed in Section 3.3, the building leakage was scaled to a BWR reactor building (i.e., 11.6 cm² for 100%/day at 0.25 psi). A factor of 10X and 100X increased that value accordingly. While 100%/day is a seemingly large amount, this leakage rate does not occur until the building pressurizes to 1723 Pa (0.25 psi), which is much, much higher than the building pressurization in the TOP scenario. Also, for reference, a 100X building leakage (i.e., 0.116 m² /180 in²) is equivalent to a 0.5 cm gap around a 6-m x 6-m equipment access door. Similarly, an external wind will increase the building infiltration and exfiltration. Wind effects are included in DOE nuclear facility analyses due to the low internal building driving forces for leakage [13].

The iodine environmental release results in Figure 4-8 illustrate mechanisms that can reduce the reactor building retention. The solid blue line is the base response. As additional leakage and wind is added, the environmental release increases by a factor of 125 from 8x10⁻⁶ to ~10⁻³ with 100X leakage and a sustained wind speed of 10 mph. This example illustrates the use of MELCOR to explore the sensitivity of the building leakage characteristics and environmental conditions on the magnitude of the overall source term.

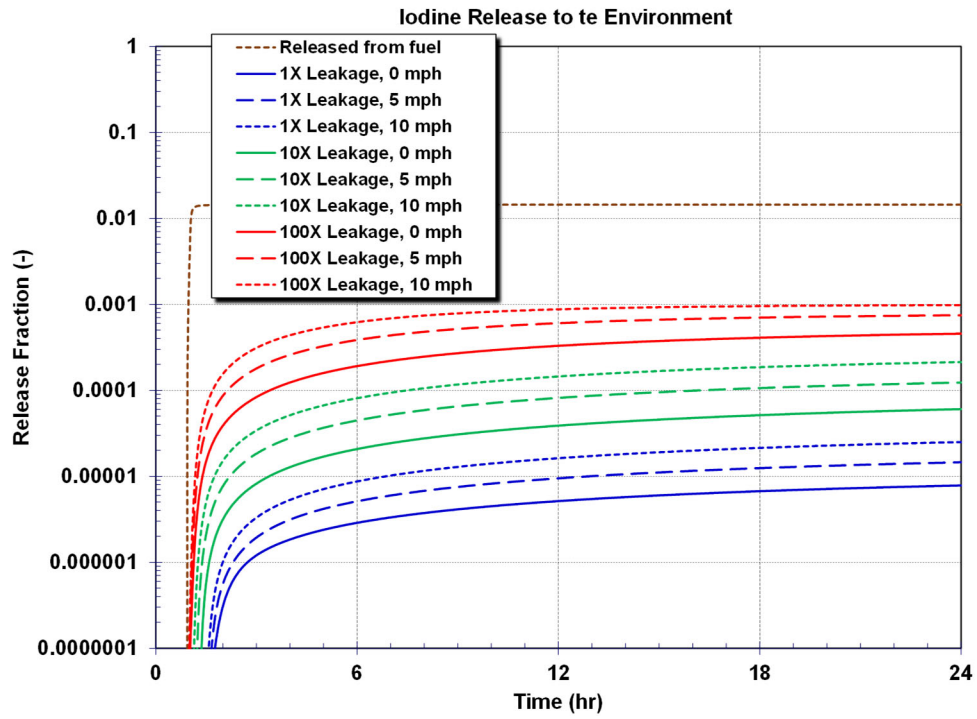


Figure 4-8 Iodine release to the environment the TOP sensitivity calculations.

Table 4-1 Uncertain parameters for the HPR.

Component	Parameter	Ranges
Heat Pipes	Heat Pipe Failure Location	Condenser (50%) / Evaporator (50%)
	Initial non-functional HPs	0% to 5%
Core	Gaseous Iodine Fraction (-)	0.0 to 0.05
	Reactivity Insertion Rate (\$/s)	0.5×10^{-4} to 1.0×10^{-3}
	Total reactivity feedback	-0.0015 to -0.0025
Vessel	Fuel Element Radial View Factor Multiplier (-)	0.5 to 2.0
	Vessel Emissivity (-)	0.125 to 0.375
	Total Leak Area (m ²)	2×10^{-5} to 2×10^{-3}
	Vessel and Vessel Upper Head HTC (W/m-K)	1 to 10
Confinement	Cavity entrance open fraction	1.0 (90%) to 0.01 (10%)
	Cavity Emissivity (-)	0.125 to 0.375
	Wind Loading (m/s)	0 to 10
	Total Leak Area Multiplier (-)	1 to 100
Scenario	Peak fuel temperature for safety rod insertion (K)	1300 to 2200

4.3. Loss-of-Heat Sink and Anticipated Transient Without SCRAM

The loss-of-heat sink (LOHS) is another postulated scenario for the HPR. In the LOHS scenario, the secondary heat removal trips off, which is followed by the actuation of the reactor shutdown system. There is no active heat removal. In a second variation, the reactor protection system does not work, or an ATWS. Figure 4-9 shows the peak and average fuel temperature responses for the two scenarios. Following the loss of the secondary heat removal, the temperature rises in both calculations but only reaches maximums of 911°C and 1036°C, respectively. Both peak temperatures show margin to cladding failure, which is assumed occur at 1377°C (i.e., near the stainless steel cladding melting temperature). The responses are slightly different with the ATWS scenario rising in temperature much more quickly whereas the LOHS has a slower response and a later peak fuel temperature.

The ATWS response includes an initial rapid temperature increase due to the additional fission power following the loss of heat removal. However, there is a strong negative reactivity feedback during the initial temperature rise. The Doppler and fuel elongation are the dominant reactivity feedbacks with the radial expansion of the reflector as a secondary effect (see Figure 4-10). The fuel heats faster (i.e., average temperature rise of 160°C by 10 min versus 95°C for the reflector) and the feedback coefficient is larger (-0.00155 $\$/^{\circ}\text{C}$ versus -0.00064 $\$/^{\circ}\text{C}$ for the reflector). The net effect is a - $\$0.31$ total feedback reactivity change over 10 min due to the rapid temperature increase. Although not included in this calculation, the xenon poisoning transient would further increase the negative reactivity feedback over the next 24 hr.

The power response for ATWS is shown in Figure 4-11. The strong negative reactivity leads to a sharp decrease in the fission power from 4.66 MW to near zero over 10 min. Only the decay heat remains after 10 minutes. MELCOR's decay heat curve is assumed constant prior to 10 min and logically coupled to the time-dependent decay heat curves when the fission power drops below 1% of full power. This starts the decrease in the decay heat following the end of the fission. Consequently, the timing of the decay power decrease in the ATWS calculation is offset from the LOHS by 10 minute. The long-term ATWS temperature response reflects a slightly faster cooldown relative to the LOHS due to the higher temperature difference to the reactor cavity during the cooldown.

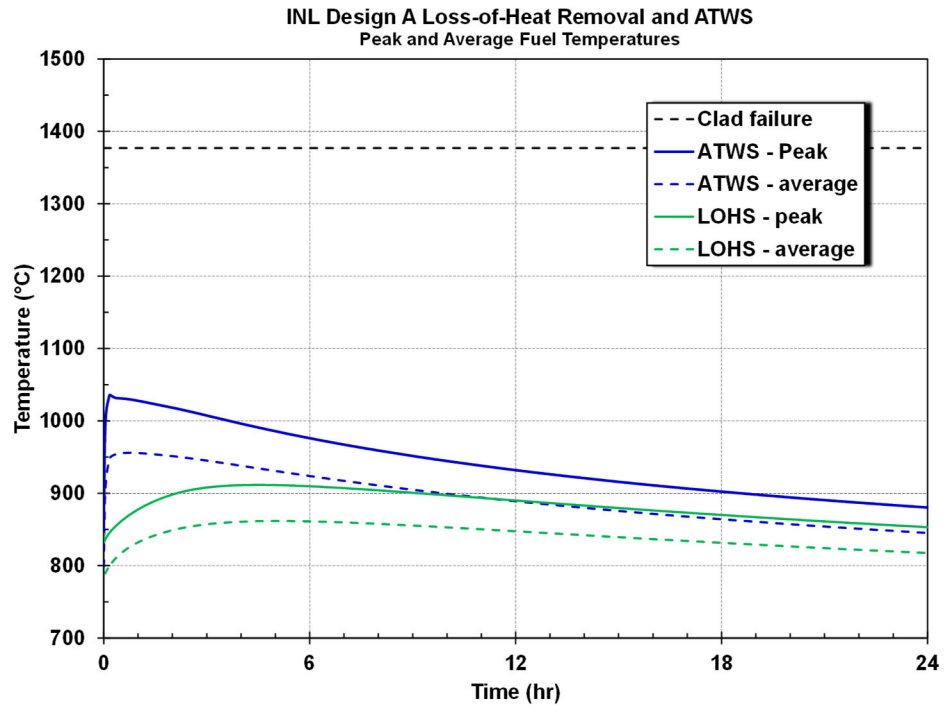


Figure 4-9 Peak fuel temperature response in the ATWS and the LOHS.

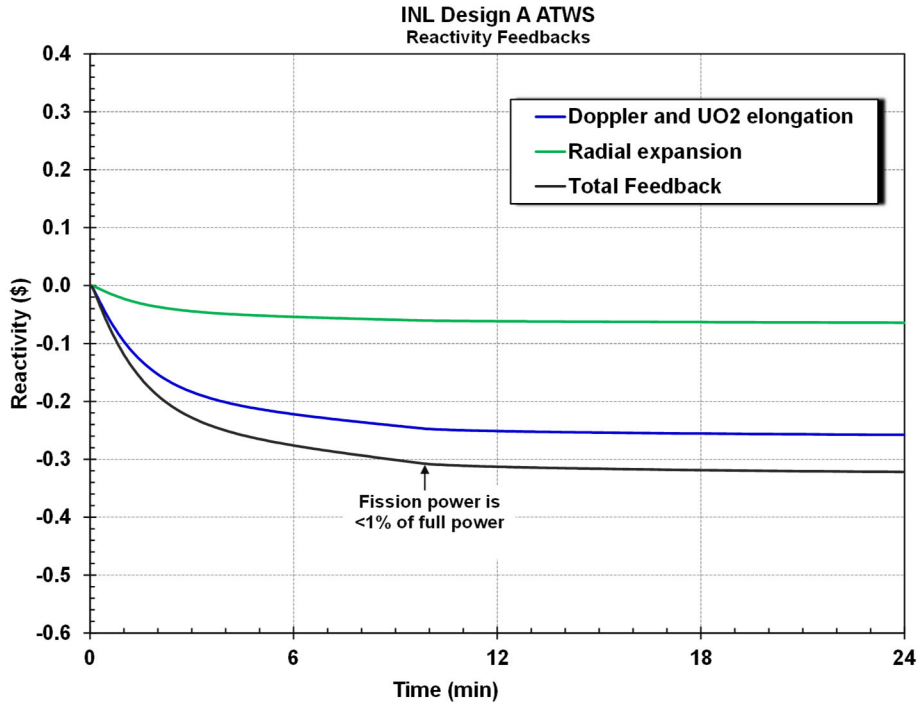


Figure 4-10 Doppler, elongation, and expansion feedbacks in the ATWS.

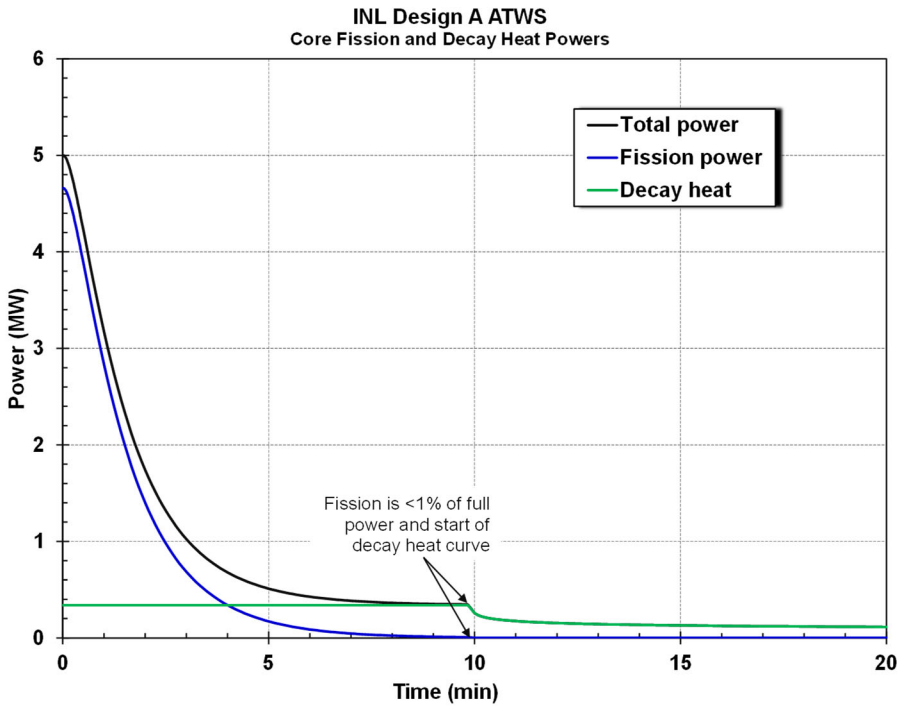


Figure 4-11 Core power and decay heat in the ATWS.

5. SUMMARY

The MELCOR code has been updated to support NRC evaluations of accidents in HPRs. This report presents demonstration calculations for a HPR design from publicly available literature. A model of the INL Design A HPR was developed to demonstrate a mechanistic source term analysis, which included the heat-pipe-cooled core, the reactor vessel, the secondary heat exchanger, and the reactor building. The HPR input model was used to simulate TOP, LOHS, and ATWS scenarios. The analyses demonstrate the flexible capabilities of MELCOR to evaluate the accident progression in an HPR. The code easily incorporates evolving data from ongoing research programs and includes flexible inputs for sensitivity and Monte Carlo sampling on uncertain parameters (e.g., see an example in the public presentation [7]).

REFERENCES

- [1] “Non-LWR Vision and Strategy Near-Term Implementation Action Plans,” Nuclear Regulatory Commission, ADAMS Accession No. ML16334A495, 2019.
- [2] “Nuclear Energy Innovation and Modernization Act,” Public Law No: 115-439, January 2019.
- [3] Humphries, L. L., et al., MELCOR Computer Code Manuals: Volume 1; Reference Manual - Version 2.2.18019, Sandia National Laboratories, SAND2019-13442, Jan 2021.
- [4] B. Rearden and M. Jessee, "SCALE Code System, ORNL/TM-2005/39, Version 6.2.3," UT-Battelle, LLC, Oak Ridge National Laboratory, 2018.
- [5] Sterbentz, James W., et al., “Preliminary Assessment of Two Alternative Core Design Concepts for the Special Purpose Reactor,” Idaho National Laboratory, INL/EXT-17-43212, Revision 1, May 2018.
- [6] McClure, Patrick R., et al., “Design of Megawatt Power Level Heat Pipe Reactors,” Los Alamos National Laboratory, 2015-11-12, LA-UR-15-28840, November 2015.
- [7] “SCALE/MELCOR Non-LWR Source Term Demonstration Project – Heat Pipe Reactor,” NRC Adams Ascension Number ML21200A179, <https://adamswebsearch2.nrc.gov/webSearch2/main.jsp?AccessionNumber= ML21179C060>, June 2021.
- [8] NASA, “Demonstration Proves Nuclear Fission System Can Provide Space Exploration Power,” <https://www.nasa.gov/press-release/demonstration-proves-nuclear-fission-system-can-provide-space-exploration-power>. May 2, 2018, Release 18-031.
- [9] Woloshun, K. A., Merrigan, M. A., and Best, E. D., HTPIPE: A Steady-State Heat Pipe Analysis Program, A User’s Manual,” Los Alamos National Laboratory, LA-11324-M, November 1988.
- [10] Cotter, T. P., “Theory of Heat Pipes,” Los Alamos Scientific Laboratory, LA-3246-MSUC-34, March 1965.
- [11] NUREG-2161, “Consequence Study of a Beyond-Design-Basis Earthquake Affecting the Spent Fuel Pool for a U.S. Mark I Boiling Water Reactor,” U.S. Nuclear Regulatory Commission, Washington, DC., September 2014.
- [12] Ananth, K. P., et al, “Portable Special Purpose Nuclear Reactor (2 MW) for Remote Operating Bases and Microgrids,” 2017 Joint Service Power Expo, May 1-4, 2017, Virginia Beach, VA, INL/CON-17-41817.
- [13] Louie, D. L., Humphries, L. L., “NSRD-10: Leak Path Factor Guidance Using MELCOR,” Sandia National Laboratories, SAND2017-3200, March 2017.
- [14] ASHRAE, “Handbook of Fundamentals,” American Society of Heating, Refrigerating and Air-Conditioning Engineers, Inc, 1997.
- [15] Walker, E., “SCALE Modeling of the Fast-Spectrum Heat Pipe Reactor,” Oak Ridge National Laboratory, ORNL/TM-2021/2021, July 2021.
- [16] “State-of-the-Art Reactor Consequence Analysis Project Volume 2: Surry Integrated Analysis.” U.S. Nuclear Regulatory Commission, NUREG/CR-7110, Volume 2, Rev. 1, January 2012.

- [17] NUREG/CR-7155. “State-of-the-Art Reactor Consequence Analyses Project, Uncertainty Analysis of the Unmitigated Long-Term Station Blackout of the Peach Bottom Atomic Power Station.” U.S. Nuclear Regulatory Commission, Washington, DC. May 2016.
- [18] NUREG/CR-7245, “State-of-the-Art Reactor Consequence Analyses Project: Sequoyah Integrated Deterministic and Uncertainty Analysis.” U.S. Nuclear Regulatory Commission, Washington, DC. October 2019.
- [19] NUREG/CR-7262 (DRAFT). “State-of-the-Art Reactor Consequence Analyses Project: Uncertainty Analysis of the Unmitigated Short-Term Station Blackout of the Surry Power Station.” U.S. Nuclear Regulatory Commission, Washington, DC. August 2019.
- [20] NUREG/CR-7110, Volume 1, Rev. 1. “State-of-the-Art Reactor Consequence Analysis Project Volume 1: Peach Bottom Integrated Analysis.” U.S. Nuclear Regulatory Commission, Washington, DC. January 2012.
- [21] Gauntt, R. O., “Synthesis of VERCORS and Phebus data in Severe Accident Codes and Applications,” SAND2010-1633, Sandia National Laboratories, April 2010.

DISTRIBUTION

Email—Internal

Name	Org.	Sandia Email Address
David Luxat	08852	dlluxat@sandia.gov
Brad Beeny	08852	babeeny@sandia.gov
Technical Library	01911	<u>sanddocs@sandia.gov</u>

Email—External (encrypt for OUO)

Name	Company Email Address	Company Name
Jason Schaperow	jason.schaperow@nrc.gov	NRC
Hossein Esmaili	hossein.esmaili@nrc.gov	NRC

Hardcopy—Internal

Number of Copies	Name	Org.	Mailstop

This page left blank



**Sandia
National
Laboratories**

Sandia National Laboratories is a multimission laboratory managed and operated by National Technology & Engineering Solutions of Sandia LLC, a wholly owned subsidiary of Honeywell International Inc. for the U.S. Department of Energy's National Nuclear Security Administration under contract DE-NA0003525.